Dynamic response patterns of profile soil moisture wetting events under different land covers in the Mountainous area of the Heihe River Watershed, Northwest China

Jie Tian[a], Baoqing Zhang[a*], Chansheng He[a,b*], Zhibo Han[a], Heye Reemt Bogena[c], Johan Alexander Huisman[c]

a Key Laboratory of Western China's Environmental Systems (Ministry of Education), College of Earth and Environmental Sciences, Lanzhou University, Lanzhou, Gansu 730000, China

b Department of Geography, Western Michigan University, Kalamazoo, MI 49008, USA

c Agrosphere Institute (IBG-3), Forschungszentrum Jülich, 52425 Jülich, Germany

PostPrint for Self-archiving. Full publication is:

Tian, J., B. Zhang, C. He, Z. Han, H.R Bogena, and J.A. Huisman. 2019. Dynamic response patterns of profile soil moisture wetting events under different land covers in the Mountainous area of the Heihe River Watershed, Northwest China. Agricultural and Forest Meteorology, 271, 225-239.

* Corresponding to: Baoqing Zhang (baoqzhang@lzu.edu.cn); Chansheng He (cshe@lzu.edu.cn)

ABSTRACT

Understanding the dynamic response of soil moisture to rainfall is critical for hydrological modelling in arid and semi-arid basins. However, little is known about rainfall-related soil moisture dynamics in arid high-altitude mountainous areas due to the absence of long-term high-resolution soil moisture observations. In this study, we investigated the dynamic response processes of profile soil moisture using data from a soil moisture monitoring network in the Qilian Mountains established in 2013 covering altitudes from 2,000 - 5,000 m a.s.l. To investigate the effects of different land covers on soil moisture response, we selected data from eight soil moisture stations with the same soil textural class and slope, but different land covers (scrubland, meadow, high coverage grassland (HCG), medium coverage grassland (MCG) and barren land). Several indices were evaluated to quantitatively describe soil moisture dynamics during the growing seasons of 2014 - 2016 based on soil wetting events. In addition, HYDRUS-1D simulations were used to further analyze the effect of land cover on soil moisture dynamics. Our results showed that soil moisture response amplitudes along profile are similar under MCG and barren land, but significantly different under scrubland, meadow and HCG. The rate of soil moisture increment decreased significantly with depth for all land covers, except for the HCG. The temporal pattern of soil moisture increase was highly variable along the soil profiles depending on land cover type. In particular, the difference of response time between the adjacent layers varied from negative values to 280 hours with depth. Preferential flow occurred mostly in soils covered by scrubland. Water transferability was higher in deeply rooted soil.

Furthermore, sensitivity analysis indicated that soil hydraulic properties are key factors in regulating profile soil wetting events. Our results show that the soil moisture response indices are useful to quantitatively characterize patterns in profile soil moisture dynamics, and provide new insights into the soil moisture profile wetting process (e.g. occurrence of preferential flow etc.), which helps for effective model parameterization and validation, in turn improving hydrological modelling in arid high-altitude mountainous areas.

KEY WORDS: Soil moisture response pattern, land cover, Heihe River Watershed, high-altitude mountainous area

1. Introduction

Mountain areas are the "water towers" of the world because of their importance in providing water resources for downstream areas (Immerzeel et al., 2010). Mountain areas provide up to 95% of the freshwater supply in some areas (Liniger et al., 1998), such as the arid and semiarid watersheds in northwestern China (Cheng et al., 2014). Soil moisture is an essential variable in hydrology, meteorology, agriculture, and ecology (Western et al., 2004; Seneviratne et al., 2010; Jung et al., 2010). Soil moisture and its dynamic response to rainfall control the interaction among the hydrological processes of precipitation, infiltration, evapotranspiration, runoff and drainage (Koster et al., 2004; Zehe et al., 2005; Wang et al., 2012a; Farrick et al., 2014; Vereecken et al., 2015). Thus, knowledge about the processes driving rainfall-related soil moisture dynamics is essential to understand the mechanisms of rainfall-runoff processes, and to improve land surface and hydrological modeling, especially in data-scarce mountainous catchments (Blume et al., 2009; He et al., 2012; McDonnell and Beven, 2014).

In recent years, mountain areas have received growing attention in the context of climate change and adaptation studies and water resources management (Lutz et al., 2014; Chen et al., 2016; Ran et al., 2018). However, the dynamics of soil moisture response to rainfall is still poorly investigated in high mountain areas (He et al., 2012; Pellet and Hauck, 2017). For example, many studies have focused on understanding the soil moisture response to rainfall. Most of these studies explored the dynamic response through qualitative description of time series of soil moisture (Kim et al., 2009; Li et

al., 2013a; Yu et al., 2015) and descriptive statistics for the specific status of soil moisture (e.g. probability distributions (Laio et al., 2001; Liu et al., 2015), and standard deviation (Rosenbaum et al., 2012; Brocca et al., 2014)). A process-based understanding of soil moisture response to rainfall remains incomplete and is urgently needed for advancing ecohydrological and critical zone modelling (Green and Erskine, 2011; Clark et al., 2017; Li et al., 2017; Guo and Lin, 2018). Moreover, quantification of soil moisture response processes using continuous in-situ monitoring data at different depths with high temporal resolution can provide alternative metrics for process-based soil hydrological model evaluation (Green and Erskine, 2011; Wiekenkamp et al., 2016; Guo and Lin, 2018).

Land cover change is known to have strong influence on soil moisture dynamics after rainfall by altering interception (Laio et al., 2001; Li et al., 2013a), infiltration (Rossi et al., 2018; Liang et al., 2011; Brooks et al., 2015), plant water uptake (He et al., 2013; Kurc and Small, 2004), and evaporation processes (Farmer et al., 2003; Jian et al., 2015). However, uncertainty remains about the soil water response regime for land cover types under different conditions (Moran et al., 2010; Li et al., 2013a; 2018b). For example, many studies showed a more dynamic soil moisture response regime under grassland than scrubland or woodland (Wang et al., 2013; Wang et al., 2008; Yu et al., 2017; Lozano-Parra et al., 2015; Li et al., 2013a). Other studies, however, showed a more dynamic response regime under scrubland or woodland than grassland (Jin et al., 2018; Li et al., 2013a; Liang et al. 2011), and some studies also found similar

response patterns for different land covers (Moran et al., 2010; He et al., 2012; Zhu et al., 2014). Furthermore, understanding of profile soil moisture response processes during and after rainfall is still unclear (Jin et al., 2018), which is vital for the detection and understanding of subsurface flow (Green and Erskine, 2011; Wiekenkamp et al., 2016; Guo and Lin, 2018) and runoff generation (Blume et al., 2009; Kim, 2009).

The response regimes under different land covers are particularly poorly understood in data-scarce mountainous areas due to the difficulties of installing and maintaining long-term profile soil moisture monitoring networks with high time resolution (Pellet and Hauck, 2017; Viviroli et al., 2011). Amongst the numerous established long-term soil moisture monitoring networks (e.g. Dorigo et al., 2011; Ochsner et al., 2013; Quiring et al., 2016; Gasch et al., 2017), only a few networks have been established in high and cold mountain areas (Su et al., 2011; Pellet and Hauck, 2017; Li et al., 2013b; Li et al., 2018). Only a few studies have focused on rainfall-related soil moisture dynamics processes for land cover types at small scale in the high and cold mountain areas (He et al., 2012; Sun et al., 2015; Yang et al., 2017). Meanwhile, the transfer of small-scale information to larger scales remains very challenging due to the high heterogeneity of soil moisture in topographically complex mountainous areas (Brocca et al., 2010; Thompson et al., 2011; Famiglietti et al., 2008).

Within this context, the aim of this study is to quantitatively describe the patterns of rainfall-related profile soil moisture response processes for typical land covers in a high-altitude, topographically complex alpine region using data from a long-term large-

scale soil moisture monitoring network. The results are expected to shed insights into rainfall-related profile soil hydrological processes under typical land covers, and to provide important reference values for key parameters in large scale hydrological modelling and water resources management in arid and semi-arid watersheds.

2. Study Area, Datasets and Methods

2.1. Study area

The Heihe River Watershed is the second largest inland river watershed (or terminal lake) in China (Cheng et al., 2014). The upper stream of the Heihe River Watershed was selected as our study area. It is located in the Qilian Mountains at the northern margin of the Qinghai-Tibet Plateau with an area of about 27×10^3 km^2 (97°29′-101°32′ E, 37°43′-39°39′ N) (Fig. 1). Mountain runoff provides almost all of the water for the entire watershed, sustains a population of about 1,21 million in the watershed, irrigates 2.4×10^5 hectares of farmland for maintaining one of the major grain production bases in China, and supports a fragile ecological system in the lower reach of the Heihe River (He et al., 2009; Li et al., 2015a).

The study area is subject to a temperate semi-arid and semi-humid continental monsoon climate. Most of the study area is located between 2,000 - 5,000 m above sea level (a.s.l.). Annual precipitation ranges from 200 mm in the steppe to 700 mm high up in the mountain ranges, and is characterized by a high seasonal variability with over 60% of precipitation falling in the summer months (Li et al., 2009). The mean annual

potential evapotranspiration is about 700 - 2,000 mm (Pan and Tian, 2001). The annual average temperature ranges from -3.1 °C to 3.6 °C based on the meteorological data from 1960 to 2012 (Zhang et al., 2016). The strong vertical difference in mean annual temperature has led to a distinct vertical land-cover zonation that comprises alpine meadow, grassland, shrub land, sparse vegetated land, and forest (Yang et al., 2015; Zhou et al., 2016; Feng et al., 2013). The main soil types are alpine steppe soil (FAO, Calcic chernozems), chestnut soil (FAO, Kastanozems), and alpine frost desert soil (FAO, Gelicregosols) (Li et al., 2009). The main soil textural classes in the study area are silt loam, silt and sandy loam (United States Department of Agriculture or USDA classification) (Tian et al., 2017).

2.2. Soil moisture network

In order to investigate the influence of different environmental factors on profile soil moisture dynamics in the upstream of the Heihe River Watershed in the Qilian Mountain, a long-term monitoring network consisting of 32 soil moisture stations has been established since July 2013 (Fig. 1). The locations of the soil moisture stations were chosen to be representative of the main land cover and soil types as well as the different altitude levels of the study area (Jin et al., 2015; Zhang et al., 2017a). The network constitutes the best possible coverage of the study area given the constraints of steep topography, rough and dangerous road conditions, accessibility to the monitoring stations, as well as financial resources (Fig. 1).

At each station, a soil pit of sufficient size was dug to enable insertion of the soil moisture sensors in multiple depths. The combined soil moisture and temperature probe ECH20 5TE (Decagon Devices Inc., Pullman, USA) was installed horizontally at depths of 5, 15, 25, 40 and 60 cm below the soil surface. The 5TE sensors were installed in such a way to avoid influence on the vertical water flow (Lozano-Parra et al., 2015). After installation, the pit was carefully refilled with the original soil material and compacted to the original bulk density layer by layer to avoid perturbations as much as possible. The soil profiles were divided into five layers according to the installation depths of the five sensors (layer 1: 0-10 cm; layer 2: 10-20 cm; layer 3: 20-30 cm; layer 4: 30-50 cm; layer 5: 50-70 cm). Soil moisture was measured at a temporal resolution of 30 min, which is in most cases sufficient to study soil hydrological processes (Lozano-Parra et al., 2015). Soil samples for each soil moisture monitoring station were collected during installation (more than 7 kg from each profile of each stations) and taken to the lab for calibration. A soil-specific calibration was carried out for each station following the step-by-step instruction guide in the manual provided by Decagon (Cobos and Chambers, 2010; Zhang et al., 2017a).

Regular station maintenance (e.g. data collection, battery and sensor check and replacement) took place twice a year at the beginning of June and at the end of October. However, the large scale of the area and the harsh mountainous environment are challenging for soil moisture network maintenance. In addition, wireless data transmission was not possible as the study area is not covered by a mobile

182 communication network. Therefore, some data gaps occurred due to battery or sensor
183 failures and damages due to livestock (sheep and yaks) and rats.

184 In order to study the soil moisture regimes under different land covers, we selected
185 a subset of stations from the entire soil moisture network with different land covers,
186 similar soil texture (silt loam, which is the main soil texture in the study area (Zhao et
187 al., 2014; Su et al., 2011)), small slope (0-9°), and with data gaps smaller than 3 months
188 in the period 2014-2016. Based on these criteria, eight typical soil moisture stations
189 were selected for this study that included the land covers of scrubland (one soil moisture
190 station, with gap from 7.2014 to 9.2014 at layer 4), meadow (one station, with gap
191 during 6.2015 at layer 5), high coverage grassland (two stations, with gap during 9.2014
192 at layer 1), medium coverage grassland (two stations, no gaps) and barren land (two
193 stations, no gaps). The locations of the selected soil moisture stations are shown in Fig.
194 1. Additionally, table 1 and Table A1 present the basic characteristics and soil properties
195 of the soil moisture stations. Here, we analyze soil moisture observations from the
196 growing seasons from May to October of 2014 to 2016 (Liu et al., 2015) (Fig. 2).

197 During the installation of the soil moisture sensors, undisturbed and disturbed soil
198 samples were taken using metal cylinders and self-sealing bags, respectively. The soil
199 samples were used to determine key soil properties for each soil moisture station (i.e.
200 saturated hydraulic conductivity, soil water retention function, soil texture, soil bulk
201 density and soil organic carbon content). Other station-related parameters include land
202 cover type (i.e. scrubland, meadow, high coverage grassland, medium coverage

grassland, and barren land), slope, aspect, slope position, and rooting depth. A detailed description of the soil properties is given in Tian et al. (2017).

Soil water retention curves were determined using the centrifuge method (KOKUSAN-H-1400pF, Kokusan Corp., Tokyo; Reatto et al., 2008). The total soil porosity was calculated from soil bulk density by assuming a particle density of 2.65 g cm^{-3} (McKenzie et al., 2002). The Mualem-van Genuchten parameters of the soil water retention curve (Van Genuchten, 1980) were fitted to the measured data using Matlab (MathWorks, Inc., Massachusetts) (Fig. 3).

2.3. Precipitation Data

Rainfall observations in the Qilian Mountains are sparse (Yang et al., 2013; Chen et al., 2014a). Therefore, we established four additional meteorological stations in the study area in September 2013. Furthermore, we used rainfall data from eight meteorological stations operated by the Heihe Ecohydrological Remote Sensing Experiment (http://www.heihedata.org/data). However, the representativeness of these meteorological stations is still limited for our study given the large area of the soil moisture network and the strong spatial variability of precipitation in the topographically complex mountainous area (Pan et al., 2014; Zhang et al., 2017b). Thus, the reanalysis datasets of Xiong and Yan (2013) and Zhang et al. (2018) (http://westdc.westgis.ac.cn) were also used in our study (Fig. 1). Throughout this study,

222 the rainfall data were used as a reference in the process of identifying the soil moisture
223 response events (Dorigo et al., 2013).

224 *2.4. Data analysis*

225 It is assumed that water reaches a certain depth when the soil moisture content
226 begins to increase after a rainfall pulse (Wang et al., 2008; Laio et al., 2001; Green and
227 Erskine, 2011). Accordingly, the soil wetting process after a rainfall was determined
228 and characterized using the increase of soil water content at depths of 5, 15, 25, 40 and
229 60 cm along the soil profile in this study (Lozano-Parra et al., 2015). Prior to the data
230 analysis, a detailed data quality control was performed following the procedures of
231 Dorigo et al. (2013), Rosenbaum et al. (2012) and Wiekenkamp et al. (2016). The data
232 quality control uses rainfall information and the measured soil temperature data and
233 consisted of the following steps. First, soil moisture data during seasonal freeze-thaw
234 periods were excluded based on soil temperature data and the characteristic soil
235 moisture dynamics in thawing and refreezing cycles (Dorigo et al., 2013; Wang et al.,
236 2017; Wang et al., 2012b; Yang et al., 2017). Second, outliers were removed using
237 quantitative plausibility checks (values outside of 0-90 vol. % range, spikes and
238 unreasonable fluctuation). Third, unreliable data caused by technical problems (e.g.
239 insufficient battery power) were eliminated by visual data inspection. Fourth,
240 temperature effects on the soil moisture data were corrected based on the methods of

241 Saito et al. (2009; 2013), in which calibration equations were derived using daily
242 fluctuations of soil water content (θ) and soil temperature (T).

243 *2.5. Identification of soil wetting events*

244 In this study, we adopted the concept of soil wetting events, which are defined as
245 events in which a significant increase of soil moisture as a result of rainfall infiltration
246 into the soil can be observed (McMillan and Srinivasan, 2015; Lozano-Parra et al.,
247 2015). To this end, we determined "critical points" in each soil moisture time series, i.e.
248 turning points indicating the beginning and end of the wetting processes (see Fig. 4),
249 and subsequently analyzed time lag and extent of the soil moisture increase. The
250 identification of the critical points was performed automatically using a dedicated
251 Matlab script. Following Lozano-Parra et al. (2015; 2016), we defined an increase in
252 soil moisture of more than 0.3% as a soil wetting event in order to consider the
253 measurement accuracy of the soil moisture sensors. Furthermore, we used a period of
254 6 hours without effective soil moisture increment as a separation criterion to distinguish
255 soil wetting events in our study (Lozano-Parra et al., 2015; 2016). An example of a
256 detected soil wetting event at two depths is presented in Fig. 4.

257 *2.6. Quantification of the response pattern of soil wetting events*

258 Based on the observed soil wetting events, we evaluated a set of indices to
259 quantitatively describe the soil moisture response and to investigate its distribution

along the soil profile for different land covers. In the following, we present the derivation of these indices in detail.

The degree of soil moisture response to a rainfall event has been analyzed by numerous soil moisture indices. For instance, McColl et al. (2017) developed a soil moisture index in which only the positive soil moisture increments during a rainfall event are considered. On the other hand, Liang et al. (2011) analyzed the maximum change in soil moisture during rainfall events by summing up the positive and negative soil moisture increments during a rainfall event. In our analysis, we define the absolute accumulated increase in soil moisture at each measurement location as follows:

$$ASWI^j = \sum_{t=ST}^{ET} \Delta\theta_{t+}^j, \quad (1)$$

with

$$\Delta\theta_{t+}^j = \begin{cases} \Delta\theta_t^j, & \Delta\theta_t^j > 0 \\ 0, & \Delta\theta_t^j \leq 0 \end{cases} \quad (2)$$

where $\Delta\theta_t^j = \theta_{t+\Delta t}^j - \theta_t^j$, θ_t^j is the volumetric soil water content (vol.%) at the time t of the jth rainfall event, Δt is the measurement interval (30 min), ST and ET are the start and end time of the jth soil wetting event, and ASWI is the accumulated soil water increment for a soil wetting event (i.e. the ASWI derived from the event shown in Fig. 4 for layers 1 and 2 is 17.47% and 3.06%, respectively). ASWI was calculated for all soil wetting events and for all measurement locations and subsequently aggregated across the stations for each land cover type. In addition, we calculated the ratio of ASWI between adjacent soil layers (RSWI) for the corresponding soil wetting events as:

$$RSWI_i^j\ (\%) = 100 \times ASWI_{i-1}^j / ASWI_i^j \qquad (3)$$

where i represents the soil layer (i = 2, 3, 4, 5), $ASWI_{i-1}^j$ and $ASWI_i^j$ are the accumulated soil water increments of layers $i-1$ and i during the period of the jth soil wetting event at layer i, respectively. The RSWI of layer 2 for the event shown in Fig. 4 is 17.54%.

The rate of soil wetting is a quantitative index which has been used to characterize the type of infiltration process (Lozano-Parra et al., 2016), and for the calibration of soil hydrology models (Green and Erskine, 2011; Laio et al., 2001). It considers the maximum and mean slope of the soil wetting curve and is based on the time derivative of the soil water increase:

$$S_{\max} = \max(100 \times \frac{\theta_{t+\Delta t} - \theta_t}{\Delta t}) \qquad (4)$$

$$S_{\text{mean}} = \text{mean}(100 \times \frac{\theta_{t+\Delta t} - \theta_t}{\Delta t}) \qquad (5)$$

where S_{max} and S_{mean} are the maximum and mean rate or slope of a soil wetting curve ($100 \times \Delta\text{vol.}\%/\text{min}$), respectively. The $S_{\max}$ and S_{mean} derived from the event shown in Fig. 4 for layer 1 is 34.96 and 3.88, respectively, while they are 0.81 and 0.44 for layer 2.

According to Sun et al. (2015), the temporal pattern of soil wetting during the infiltration event can be divided into the period between the start of a rainfall event and the start of the corresponding soil moisture response (also known as the soil moisture response time) and the period of soil moisture increase (i.e. the duration of the soil

301 wetting event). Quantitative descriptions of these two periods can provide new insights
302 into the temporal patterns of the soil wetting process along a soil profile.

303 The difference of the soil moisture response time (DRT) between two adjacent soil
304 layers was evaluated to characterize the temporal delay of the soil wetting events with
305 depth (Sun et al., 2015; Li et al., 2015b; Germann and Hensel, 2006). It is calculated as:

306 $$DRT_i = ST_i - ST_{i-1} \quad (6)$$

307 where ST_{i-1} and ST_i are the response times of layer $i-1$ and i to a rainfall event
308 ($i = 2, 3, 4, 5$), and DRT_i is the difference of the response times (hour). The DRT for
309 the event shown in Fig. 4 is 0.5 hour for layer 2. The duration of the soil wetting process
310 (h) for a specific soil layer is calculated as:

311 $$\text{Duration}_j = ET_j - ST_j \quad (7)$$

312 where ET_j and ST_j are the end and start time of the *j*th soil wetting event for a specific
313 soil layer. The duration of the event shown in Fig. 4 is 7.5 hours for layer 1 and 11.5
314 hours for layer 2.

315 Finally, based on the increment of soil wetting event, the accumulated soil storage
316 increment (ASSI) for different layers under different land covers were calculated as:

317 $$\text{ASSI}_i = \sum ASWI_i \times d_i \quad (8)$$

318 where $\sum ASWI_i$ is the sum of the accumulated soil moisture increment (vol. %) at
319 layer i, d_i (mm) is the corresponding measurement range of layer i
320 (d_1, d_2, d_3, d_4, d_5 is 100, 100, 100, 200, 200 mm, respectively, according to the
321 installation depths of the sensors). Furthermore, the ratio between the ASSI of a specific

layer and the sum of ASSI of the profile was calculated to normalize the vertical distribution of ASSI along depth. ASSI is the overall result of the partitioning of infiltration propagating through soil profile of 0-70 cm during the study period (Moran et al., 2010; Lozano-Parra et al., 2016).

2.7. Virtual simulations of soil moisture dynamics

The influence of land cover on soil moisture dynamics can be attributed both to plant characteristics (e.g. rooting depth, interception storage etc.) and soil properties that have developed in coevolution with vegetation (Jenny, 1994). Here, we use virtual simulations of soil moisture dynamics with the process-based soil hydrological model HYDRUS-1D (Simunek et al., 2005) to explore their individual roles in controlling the pattern of soil moisture dynamics. In addition, the virtual simulations serve to test the applicability of the indices used in this study. The sensitivity analysis included two different scenarios: (1) simulations of soil moisture dynamics with different soil properties but with the same crop parameters; (2) simulations with different crop parameters but with the same soil properties. Both scenarios were simulated using the same meteorological data.

The modified Richards equation as implemented in Hydrus-1D (Simunek et al., 2005) was used to simulate soil moisture dynamics for the two scenarios. The soil hydraulic parameters were derived by fitting the measured soil retention curve to the Mualem-van Genuchten model:

342 $$\theta(h) = \begin{cases} \theta_r + \frac{\theta_s - \theta_r}{[1+|\alpha h|^n]^m} & h < 0 \\ \theta_s & h \geq 0 \end{cases}$$

343 (9)

344 $$K(h) = K_S S_e^l \left[1 - (1 - S_e^{1/m})^m\right]^2 \quad (10)$$

345 $$S_e = \frac{\theta - \theta_r}{\theta_s - \theta_r} \quad (11)$$

346 $$m = 1 - 1/n\,, n > 1 \quad (12)$$

347 where θ_s and θ_r are the saturated and residual water content (cm^3/cm^3), respectively,
348 h is the pressure head (cm), α(1/cm) and n are empirical coefficients (which are
349 related to the air-entry value and the pore-size distribution index, respectively), and K_S
350 is the saturated hydraulic conductivity.

351 As none of the soil moisture stations includes meteorological measurements, we
352 used data from a nearby meteorological station (11 km away from the scrubland soil
353 moisture station) as climate forcing for all simulations. The potential evapotranspiration
354 was calculated by the Penman-Monteith equation within Hydrus-1D. The soil profile
355 was discretized into six materials (five soil layers matching the observations within 0-
356 0.7 m plus a soil layer extended from 0.7-2 m with the same soil properties as layer 5).
357 The lower boundary condition of HYDRUS-1D was set to free drainage since the soil
358 overlays a fractured rock system (Yao et al., 2017). The Feddes model was used for root
359 water uptake simulations (Feddes, 1978), and the vertical root distribution was
360 parameterized based on an empirical root distribution (Hoffman and van Genuchten,
361 1983) and the measured rooting depth (Simunek et al., 2005). The interception constant
362 for specific land covers were obtained by dividing the daily interception thresholds by

363 the LAI (Wang et al., 2018). The interception thresholds were obtained from the results
364 of literature values reported for the Qilian Mountains (Liu et al., 2012; Liu et al., 2013).
365 Both soil properties and crop parameters did not change during the simulation.

366 In the simulation of scenario (1), HYDRUS was applied to simulate the soil
367 moisture dynamics of the eight soil moisture stations using the measured soil properties
368 of each station, and using the same crop parameters (for scrubland). For scenario (2),
369 HYDRUS was applied to simulate soil moisture for five land cover types with their
370 respective crop parameters using the same soil properties (soil of scrubland). S_{max} and
371 Duration were calculated from the simulated soil moisture to show the applicability of
372 the indices. The soil properties and crop parameters used in the simulations are shown
373 in the supplemental material (Tables A1 and A2).

374 *2.8. Statistical analysis*

375 Descriptive statistics (maximum, minimum, mean and coefficient of variation (CV))
376 were computed for all indices and the effect of different land covers on the indices were
377 tested using a one way analysis of variance (ANOVA) (α=0.05). Least Significant
378 Difference (LSD) was used as a post-hoc-test for multiple comparisons of means
379 (α=0.05). Box-plots were used to display the distribution of index values between
380 different layers and land covers (McGill et al., 1978), and when notches do not overlap,
381 the medians can be judged to differ significantly (Muenchen, 2011; Krzywinski and
382 Altman, 2014). The statistical analysis was conducted using the SPSS statistical

383 package (SPSS 18.0, SPSS Inc., Chicago, USA) and MATLAB (MathWorks, Inc.,
384 Massachusetts, USA).

385 **3. Results**

386 The discriminated soil wetting events at each measurement location during the
387 growing season of 2014 - 2016 are summarized in Table 2. Overall, we found 1,783
388 events, of which 48 % occurred in the first soil layer and 24 % occurred in the second
389 layer. As there is only one soil moisture station each for the scrubland and meadow and
390 there are two stations for each of the other three land covers, the soil wetting events at
391 each station were aggregated within the same land cover to analyze the patterns of soil
392 wetting events under different land covers in the study area. We analyzed the soil
393 wetting events with the indices described earlier, and this analysis is summarized in
394 Table 3.

395 *3.1. Profile distribution of the increment of soil wetting event (ASWI) under different*
396 *land covers*

397 Fig. 5 and Fig. 6 show the box-plots of the derived ASWI and RSWI values for the
398 specific soil depths and land cover types, respectively. Generally, ASWI decreased with
399 depth and RSWI is below 100% in most cases, which suggests a decreasing soil
400 moisture response with increasing soil depth. Furthermore, the RSWI increased with
401 depth in most cases, suggesting that the dampening effect also reduced with depth. The

box plots of ASWI and RSWI show different reduction patterns along depth for different land covers (Fig. 5 and Fig. 6).

The scrubland shows a similar degree of soil moisture increase along the soil profile, only with a significantly decrease of ASWI at layer 3 ($p<0.05$), which may be related to the lower K_S of layer 3 (Fig. 3). At the same time, the scrubland has the highest RSWI along the soil profile amongst all land covers, with a median higher than 50% for layers 2 and 3, and a median above 100% for layers 4 and 5. Moreover, the scrubland also shows the highest number of soil wetting events in the deeper layers (Table 2), indicating that soil covered by the scrubland exhibits a less dampened soil moisture response. This is attributed to the well-developed root system, which is associated with better conditions for infiltration (Fig. 3) (He et al., 2012; Tian et al., 2017).

The soil moisture measurements for the meadow show a decline of ASWI from layer 1 (with a median of 4.3 vol. %) to layer 2 (with a median of 1.1 vol. %), which is significant at $p<0.001$, with the corresponding lowest RSWI (with a median of 17%) at layer 2. This also led to higher soil water contents in layer 1 (Fig. 2). The high RSWI at layer 5 (with median of 77%) can be partly affected by the accumulation of lateral flow from the upslope, as this soil moisture station is located at the bottom of a slope. These findings indicate that the meadow stations show a significantly higher degree of soil moisture response from layer 1 to layer 2, while there are no significant differences from layer 2 to layer 5.

422 The High coverage grassland (HCG) and Medium coverage grassland (MCG) also
423 show a significantly different degree of response along depth, while the barren land has
424 a similar degree of response along depth. The HCG has a lower RSWI than the MCG
425 in the shallow soil layers (median of 26% versus 61% at layer 2), while the HCG has a
426 higher RSWI for the deep soil layers than the MCG (median of 57% and 41% of layer
427 5 for the HCG and MCG, respectively). In addition, the extreme values of ASWI are
428 more frequent along the profile for the HCG than the MCG and barren land. This
429 indicates that the grassland stations with more vigorous vegetation consume more water
430 in the shallow soil layers, and have a better capacity to transfer water into deeper soil
431 layers.

432 Overall, the results of the multiple comparisons show a similar degree of soil
433 moisture response along depth for the scrubland ($p>0.01$) and barren land ($p>0.05$),
434 suggesting a slightly dampened pattern of response amplitude for these two land covers.
435 In contrast, the meadow, HCG and MCG stations show a heavily dampened soil
436 moisture response amplitude with depth ($p<0.01$), which is strongest for the meadow
437 station.

438 *3.2. Profile distribution of the rate of soil wetting (S_{max}, S_{mean}) for different land covers*

439 In Fig. 7, both the maximum and mean rates (S_{max} and S_{mean}) of the five soil layers
440 are shown for all five land covers. As the rates vary in a wide range, box plots of S_{max}
441 and S_{mean} are shown with a logarithmic axis. Results of Welch's ANOVA showed an

442 overall significant reduction ($p<0.01$) of rate with depth for all the land covers. The
443 maximum and mean rates of soil moisture increase showed a similar variation with
444 depth under the same land cover.

445 The scrubland showed the highest rate for the deep soil layers (with a median of 0.5
446 of S_{max} at layer 5, supposing a variation of 0.15 vol. % in 30 min at layer 5). This is
447 attributed to the fact that the scrubland has more macropores and higher K_S (Fig. 2).
448 The meadow showed the strongest reduction in rate from layer 1 (with a median of 4.86,
449 S_{max}) to layer 2 (with a median of 1.2, S_{max}), similar to the variation of response degree.

450 The HCG showed a significant higher rate at layer 1 (median of 2.4, matching a
451 variation of 0.72 vol. % in 30 min, S_{max}), followed by a stably lower range of rates from
452 layer 2 to layer 5 (median varied from 0.14 to 0.78, S_{max}). Unlike the degree of soil
453 moisture response (ASWI), the rate of soil moisture increase showed a significant
454 reduction from layer 1 to layer 3 for the MCG and barren land. This indicates that the
455 MCG and barren land have a similar response amplitude but a different response rate
456 along depth. Similar to ASWI, the extreme values of the rate are more frequent along
457 the profile for the scrubland and HCG than for the MCG and barren land, corresponding
458 to the increasing vegetation degradation (Fig. 7).

3.3. Profile distribution of temporal pattern of soil wetting event under different land covers

The temporal patterns of the soil wetting process at a specific layer along the profile are presented as the vertical variation of the response time and the duration of the wetting process in Fig. 8, Fig. 9 and Table 3.

3.3.1 Profile distribution of the response time under different land covers

The results presented in Fig. 8 show that the differences in the response time (DRT) ranged from negative values (indicating preferential flow; Wiekenkamp et al., 2016; Lin and Zhou, 2008) to as large as 270 hours in the barren land. The vertical distribution of DRT for different land covers is different to that of ASWI and rate (Fig. 8). The average DRT for each land cover increased in the order of scrubland (with a median value for the whole profile of 0.5 hours), meadow (2 hours), HCG (4 hours), MCG (7.5 hours), and barren land (16.5 hours), again corresponding to the degree of vegetation degradation in the study area (Fig. 8). The DRT increased significantly with depth for all the land covers except the HCG (Fig. 8).

The negative DRT along the profile in combination with the high RSWI (around 100%) and the relatively high rate of soil moisture increase along the profile indicates that the scrubland is influenced by preferential flow along the profile through biological macropores (worm holes or root remnants, with a range of rooting depth>70 cm). In the soil profiles under meadow, bypass flow was not observed between layer 1 and 2 (as the DRT2 is larger than 0 hour), possibly due to the presence of the “mattic” epipedon.

For MCG, bypass flow is more frequent between layers 1 and 2, and this occurrence of bypass flow coincides with the observed range of rooting depth (within 25 cm according to the field survey, Tian et al., 2017). Bypass flow was still observed for layer 4 under HCG, which also coincides with the observed range of rooting depth (within 40 cm). In contrast, bypass flow was not observed under barren conditions (with a minimum DRT of 0.5 hours for layer 2, Fig. 8).

3.3.2 Profile distribution of the duration of soil wetting process under different land covers

The vertical pattern of duration showed a wide range of time scales for the soil wetting events under different land covers, and it varied from a median value of 6.5 hours to 170 hours (Fig. 9). The scrubland showed relatively homogenous soil wetting duration along the soil profile with a median value of 6.5 hours in the first two layers and around 14 hours in layers 3 to 5. In contrast, the wetting duration of the meadow soil profile is non-uniform, ranging from 3.5 hours (median) in the first layer to more than 40 hours (median) in the deeper soil layers. For HCG, the wetting duration extended from 8 hours to 46 hours (median value) with increasing depth. This pattern was also found for MCG and barren land, and was even more pronounced with about 10 hours (median) in the first layer to a long time scale of over 130 hours (5 days, median) in the deep layers (Fig. 9).

In summary, our results indicate that the duration of soil wetting events in the Qilian Mountain region can last from a few hours to several weeks depending on land cover,

501 soil depth and soil properties. Also, the amplitude, rate and DRT of the soil wetting
502 events varied with land cover types, soil depth and soil properties.

503 *3.4. Profile distribution of the accumulated soil wetting events under different land*
504 *covers*

505 From the proportion of ASSI (Fig. 10 (c)), we can see that the first layer showed
506 the highest proportion along the profile for all the land covers. The highest value of 80%
507 was found for the meadow, the lowest value of 30% for the scrubland, and 50-65% for
508 the other land covers. The results also show that the scrubland has a relatively even
509 distribution pattern of the proportion of ASSI with depth, while the accumulated
510 proportion of ASSI in the upper soil layers increased from HCG (with an accumulated
511 proportion of 82% at layer 3), MCG (87%) to barren land (95%). These results indicate
512 that the active soil depth involved in the infiltration processes decreased with vegetation
513 degradation in the study area, except for the meadow.

514 This can also be seen from the number of soil wetting events. The scrubland showed
515 a stable reduction of the number of soil wetting events with depth, while the barren land
516 showed a high proportion (more than 65%) of soil wetting events in layer 1. The
517 meadow, HCG, and MCG had a percentage of nearly 50% of the soil wetting events
518 recorded at layer 1 (Fig. 10 (d)). At the deepest layer, the percentage of the recorded
519 soil wetting events decreased in the following order: scrubland (11.4%), HCG (5.8%),
520 meadow (2.9%), MCG (2%), and barren land (1.6%), corresponding to the decrease of

the rooting depth of the different land covers, suggesting that land covers with a deeper root zone have more soil moisture response events at deep layers.

3.5. Simulation of the effect of land cover on soil wetting events

Based on the results above, the profile pattern of soil wetting events (increment, rate, DRT and duration) was influenced by different land covers. However, as stated above, the influence of land cover on soil wetting events can be the combined effect of both the different plant characteristics and soil properties that have developed in coevolution with vegetation, which cannot be distinguished from the observations only. Thus, the individual roles of plant characteristics and soil properties in regulating the soil wetting events were further explored through the sensitivity analysis using HYDRUS-1D.

3.4.1 Model validation

A comparison of the measured and simulated soil moisture for the scrubland is used to validate the simulation results (Figs. A1 and A2 in Supplementary material). We only validated for scrubland as this station is relatively close to a meteorological station (11 km), while the distance between meteorological stations and the other soil moisture stations is much greater. Given the strong variability of precipitation in this mountainous area, the validation for other stations was deemed to be unreliable. The correlation coefficient and RMSE for layer 1 (0.65, 0.048), layer 2 (0.67 and 0.045), layer 3 (0.67 and 0.069), layer 4 (0.81 and 0.029) and layer 5 (0.89 and 0.031) indicate

a relatively good fit. Although there is bias between the measured and simulated soil moisture, the HYDRUS-1D model was able to simulate the soil moisture trends reasonably well. An important reason for the remaining difference is the still considerable distance between the meteorological and the soil moisture station (11 km). A further explanation for the remaining deviations could be related to the strong heterogeneity of soil hydraulic properties under scrubland (Rossi et al., 2018).

To further validate the simulation results, the profile distribution of soil wetting events (SWE) for the observed and simulated time series were also compared. Fig. A2 shows that both the profile distribution of the proportion of SWI and ASSI were higher for the simulations (45%, proportion of SWE number at layer 1) than for the observations (31.3%) in the surface layer, and lower for the simulations (6% at layer 5) than for the observations (11%) in deeper layers. Similarly, the comparison of the pattern of SWE also showed a higher S_{max} and S_{mean} for the simulations than for the observations at the surface layer, while S_{max} and S_{mean} for the simulations were again lower than the observations in the deeper layers. The profile distribution of Duration was similar to S_{max} (Fig. A2).

In summary, a higher amount of soil wetting events with a higher velocity of the observed soil wetting process was found in the observed time series. These results indicate that the model underestimates the water transferability especially at greater depths. This could be attributed to the influence of preferential flow, which was observed at deeper depths (from DRT at layer 5, Fig. 8) but not explicitly accounted for

562 in the HYDRUS1D simulations. Despite this shortcoming, the general characteristics
563 of the soil wetting dynamics are reasonably reproduced by the model and thus can be
564 used for sensitivity analyses.

565 *3.4.2 Sensitivity analysis*

566 The result of the sensitivity study using HYDRUS-1D simulations for the two
567 scenarios is presented in Figs. 11 and 12 (the simulated time series of the two scenarios
568 are shown in Figs. A3 and A4 in the Appendix). For scenario (1) with the influence of
569 different profile soil properties (Fig. 11), the indices showed different profile patterns
570 in both Duration and S_{max}. S_{max} decreased with depth in different ways for all model
571 runs except the barren land, while the Duration increased with depth in different ways
572 except for the barren land. For the barren land, the increase of S_{max} at layer 4 is attributed
573 to the increase of K_S from layer 3 (0.4 cm/hour) to layer 4 (1.7 cm/hour). The different
574 profile distribution of S_{max} and Duration reflect the control of soil properties on soil
575 water dynamics, which varied considerably between each soil profile (Table A1).

576 For scenario (2) with the influence of different crop parameters (Fig. 12), both S_{max}
577 and Duration showed a similar variation with depth for different land covers. Despite
578 the different plant parameters for each land cover types, S_{max} decreased and Duration
579 increased with depth for all land cover types. Furthermore, S_{max} at deeper depths
580 decreased for several vegetation types at layer 5: scrubland (with a median value of 0.4),
581 HCG (0.22), MCG (0.2) and meadow (0.17). Apparently, the value of S_{max} at layer 5

582 seems to be related to the rooting depth (Table A2), i.e. with decreasing rooting depth,
583 the value of S_{max} for layer 5 decreases.

584 In summary, soil profiles with different soil hydraulic properties (e.g. K_S, soil
585 hydraulic properties) and the same plant parameters had different profile patterns of soil
586 wetting events (Fig. 11). However, the profiles with different plant parameters and the
587 same soil hydraulic properties showed similar profile patterns of soil wetting events
588 (Fig. 12). Thus, the results of this sensitivity analysis using HYDRUS-1D show that
589 soil hydraulic properties are key factors in regulating the profile patterns of soil wetting
590 events.

591 **4. Discussion**

592 *4.1. Response patterns of soil moisture dynamics under different land covers*

593 Vegetation has been reported to alter soil hydrological processes, e.g. the
594 propagation of wetting fronts through soil profiles (Laio et al., 2001). In our study, we
595 investigated hydrological processes using long-term measurements of profile soil
596 moisture response during rainfall infiltration under different land covers based on a set
597 of indices (ASWI, RSWI, S_{max}, S_{mean}, DRT, and Duration) that may also be useful for
598 parameterization and validation of process-based soil hydrological models.

599 Scrubland has been argued to enhance infiltration capacity (Li et al., 2009; Sun et
600 al., 2015; Jin et al., 2018) or reduce infiltration capacity in soil profile (more root water
601 uptake and interception for scrubland than grassland, especially in the (semi-) arid area,

602 Wang et al., 2008; Li et al., 2013a; Lozano-Parra et al., 2015; Yu et al., 2017) through
603 complex interactions between the well-developed root system and soil water (Moran et
604 al., 2010). In our study, both the highest RSWI along the soil profile and the highest
605 rate in the deep soil layers were observed under scrubland (Figs. 6 and 7). This indicates
606 that scrubland soil exhibited a more intensive soil moisture response, both in terms of
607 degree and rate, especially at deeper depths. In addition, the high value of the ASSI
608 index (Fig. 10) indicates that scrubland soil exhibited higher infiltration capacity. On
609 the other hand, the distribution of negative DRT revealed the frequent occurrence of
610 preferential flow (Lin and Zhou, 2008; Wiekenkamp et al., 2016) in scrubland soils.
611 This is attributed to the well-developed root system of scrubland, which is associated
612 with both better soil hydraulic conditions (Fig. 3) for infiltration (He et al., 2012; Tian
613 et al., 2017) and formation of macropores that facilitate preferential flow (Li et al., 2009;
614 Jin et al., 2018). Thus, in the hydrological modelling for scrubland, the effect of
615 preferential flow needs to be considered to best represent the hydrological processes of
616 scrubland.

617 The 'mattic' diagnostic epipedon typically found at soil depths of 0-10 cm in alpine
618 meadow soils of the Tibet plateau is formed by abundant roots and their long-term
619 interaction with the soil (Zeng et al., 2013; Zhi et al., 2017). We found that this layer
620 can significantly reduce the soil hydraulic conductivity (Fig. 3) and the soil moisture
621 response (e.g. ASWI and S_{max} from layer 1 to layer 2, Figs 5 and 7), which was also
622 suggested in other studies (Wang et al., 2007; Tian et al., 2017). Accordingly, a scheme

623 of “two soil layers with a low soil hydraulic properties for the ‘mattic’ epidedon layer
624 and a high one for the deeper soil layer” was recommended in the soil hydraulic
625 parameterization of hydrological modelling under meadow. This result is also
626 consistent with experiences from hydrological model parameterization for Alpine
627 meadow soils (Della Chiesa et al., 2014).

628 The profile response patterns suggest that land covers with a deeper root zone
629 exhibit more soil moisture response events at deep layers in the study area. This result
630 coincides with other relevant studies in the Tibet plateau (Sun et al., 2015; Yang et al.,
631 2017). Thus, rooting depth is an essential control on the transfer of rainfall infiltration
632 into deeper layers of Tibet plateau soils.

633 The profile distribution of Duration of the soil moisture increases indicated that
634 there is an accumulation of soil moisture in the deep layers under MCG and barren land,
635 which was also observed by Sun et al. (2015) and Yang et al. (2017) for grassland in
636 the Qilian Mountains. The accumulation of soil moisture in deep layers was probably
637 related to the combined effects of the continuous rainfall pattern in the study area (Sun
638 et al., 2015; He et al., 2012; Yang et al., 2017) and the lower K_S of the deeper soil layers
639 (as shown in Fig. 3) that reduces downward flow (Sun et al., 2015). In addition, the
640 deeper soil layers are not penetrated by roots and thus are less affected by
641 evapotranspiration processes (He et al., 2013; Wang et al., 2015; Broedel et al., 2017).

642 *4.2. Assessing the quantitative indices for the soil wetting event pattern*

643 There are many studies dealing with the response of soil moisture to rainfall.
644 However, most studies are based on a qualitative description through visual inspection
645 of time series of soil moisture (Kim et al., 2009; He et al., 2012; Li et al., 2013a; Yu et
646 al., 2015). For instance, Yu et al. (2015) and Kim et al. (2009) suggested the existence
647 of an "inconsistent impulse type" of soil moisture response to rainfall. In this study, we
648 evaluated several indices based on the amplitude, rate (S_{max}, S_{mean}) and timing of
649 response to characterize how the profile soil moisture response responds to rainfall
650 using 3-year time series of soil moisture under different land covers.

651 The distribution of S_{max} from the soils investigated in this study was consistent with
652 results of Lozano-Parra et al. (2016) found in the region of Extremadura, Spain.
653 However, our station showed somewhat lower values for S_{max}, which may be caused by
654 the higher hydraulic conductivity of the sandy loam soil at the Spanish site (Lozano-
655 Parra et al., 2016). Our S_{mean} pattern also matched well with the results of Sun et al.
656 (2015) and Yang et al. (2017) in a small watershed within the Qilian Mountains based
657 on typical soil wetting events, indicating the validity of our results. However, our study
658 relies on the observed general patterns of soil wetting events for five different land
659 covers from longer soil moisture records (3 years) at multiple stations.

660 DRT has been used for the identification of preferential flow (Wiekenkamp et al.,
661 2016). It increased significantly with depth for all land covers except HCG in this study.
662 This indicates that the velocity of the wetting front reduced significantly as the

infiltration front propagated deeper into the soil (Green and Erskine, 2011; Yang et al., 2017; Hardie et al., 2013). However, the occurrence of preferential flow might be underestimated in this study due to the relatively long measurement interval of 30 min. Previous studies have shown that preferential flow may occur on time scales shorter than 30 min (Lin and Zhou, 2008; Graham and Lin, 2011).

4.3. Virtual simulation of soil wetting events with HYDRUS-1D

In order to explore the individual roles of plant parameters and soil properties in controlling the soil wetting events, which can't be obtained from data analysis only, the sensitivity analysis with two scenarios were conducted through HYDRUS-1D. Through the comparison of the soil wetting patterns for two simulation scenarios, we found similar response patterns of profile soil moisture for different plant parameters and the same soil (Fig. A4 and Fig. 12), while we found different response patterns when soil properties were varied for the same land cover (Fig. A3 and Fig. 11). Thus, we conclude that soil properties are a key factor for the regulation of the profile pattern of soil moisture dynamics rather than the plant parameters. The importance of soil properties in controlling soil moisture dynamics was also reported in other studies based on hydrological modelling (Bertoldi et al., 2014; Shi et al., 2015). In addition, our virtual experimental analysis illustrated that the indices used in our study are suitable to quantitatively describe and distinguish the patterns of soil moisture dynamics.

However, land cover may not have been characterized sufficiently in terms of physiological properties in the soil hydrological modelling in this study. For instance, we used the same values for the physiological parameters of the root water uptake model for all land cover types due to the lack of more detailed information for the vegetation in the study area. Furthermore, the vertical root distribution was parameterized using a general root distribution function in HYDRUS-1D (Hoffman and van Genuchten, 1983) due to the lack of measured root density profiles. Additionally, crop parameters were kept unchanged during the simulation of HYDRUS (including LAI, rooting depth and crop height). Due to this generalization, the effect of different vegetation types on the soil moisture response to evapotranspiration may have been underestimated.

Topographic factors have been recognized as an important factor in regulating soil moisture dynamics in Qilian Mountainous area (Zhao et al., 2014). In this study, stations with only mild slopes were selected to reduce such topography effects. However, the influence of topography should be investigated in future studies using detailed slope information, in situ observations and 2D or 3D hydrological simulations.

5. Conclusions

Based on a 3-year long dataset obtained from a large-scale soil moisture monitoring network in the upper reach of the Heihe River Watershed, we quantitatively analyzed

701 the patterns of the profile soil moisture dynamic response for different land covers from
702 its response amplitude, response rate and time. The main findings are:
703 (1) The scrubland, MCG and barren land have a slightly dampened soil moisture
704 response amplitude along the soil profile, while the meadow and HCG have a heavily
705 dampened response amplitude. The rate of soil moisture increases reduced significantly
706 with depth for all the land covers, except for the HCG.
707 (2) The different land covers have significantly different temporal patterns of the
708 profile soil moisture dynamics response. The vertical variation of transmit time for the
709 wetting front advancing through the adjacent layers coincides with the extent of the root
710 zone for the different land covers. In addition, soil wetting events can last from hours
711 to weeks for different soil layers of different land covers.
712 (3) Preferential flow occurred mostly in soils covered by scrubland.
713 (4) Overall, scrubland has an evenly distributed soil moisture retention capacity
714 along the profile, whereas the major soil moisture retention capacity is concentrated in
715 the top soil for other land covers, especially the meadow. The water transferability was
716 found to be higher in deeply rooted soil.
717 (5) After separating the influence of plant parameters and soil properties on profile
718 patterns of soil wetting events, soil hydraulic properties was found to be the key factors
719 explaining the observed differences in soil moisture responses.
720 The indices used in this study can be used to quantitatively describe the patterns of
721 profile soil moisture dynamics for different land covers, and to provide new insights

into the different soil hydrological regimes under different land covers. They can also supply important information for effective model parameterization and validation, and thus improving ecohydrological modelling studies in data-scarce mountainous watersheds.

ACKNOWLEDGEMENTS

The project is partially funded by the National Natural Science Foundation of China (41530752, 91125010, and 51609111), the Strategic Priority Research Program of Chinese Academy of Sciences (XDA20100102). We are grateful to the members of the Center for Dryland Water Resources Research and Watershed Science, Lanzhou University for their hard field work to collect the soil moisture data and maintain the stations in this high, cold, and hard to access mountainous area. Without their hard work, the soil moisture data presented in this paper would not have been available. We also thank the Science Data Center for Cold and Arid Regions (http://westdc.westgis.ac.cn) for providing the supported data. We are grateful to the two anonymous reviewers and the editors for their constructive comments and suggestions on this manuscript.

REFERENCES

Bertoldi, G., Della Chiesa, S., Notarnicola, C., Pasolli, L., Niedrist, G., Tappeiner, U., 2014. Estimation of soil moisture patterns in mountain grasslands by means of SAR RADARSAT2 images andhydrological modeling. J. Hydrol. 516, 245-257.

Blume, T., Zehe, E., Bronstert, A., 2009. Use of soil moisture dynamics and patterns at different spatio-temporal scales for the investigation of subsurface flow processes. Hydrol. Earth Syst. Sci. 13 (7), 1215-1233.

744 Brocca, L., Melone, F., Moramarco, T., Morbidelli, R., 2010. Spatial - temporal
745 variability of soil moisture and its estimation across scales. Water Resour. Res. 46
746 (2).
747 Brocca, L., Zucco, G., Mittelbach, H., Moramarco, T., Seneviratne, S., 2014. Absolute
748 versus temporal anomaly and percent of saturation soil moisture spatial variability
749 for six networks worldwide. Water Resour. Res. 50 (7), 5560-5576.
750 Broedel, E., Tomasella, J., Cândido, L.A., Randow, C.V., 2017. Deep soil water
751 dynamics in an undisturbed primary forest in central Amazonia: differences
752 between normal years and the 2005 drought. Hydrol. Process. 31 (9), 1749-1759.
753 Brooks, P.D., Chorover, J., Fan, Y., Godsey, S.E., Maxwell, R.M., McNamara, J.P.,
754 Tague, C., 2015. Hydrological partitioning in the critical zone: Recent advances
755 and opportunities for developing transferable understanding of water cycle
756 dynamics. Water Resour. Res. 51 (9), 6973-6987.
757 Chen, R.S., Song, Y., Kang, E., Han, C., Liu, J., Yang, Y., Qing, W., Liu, Z., 2014a. A
758 cryosphere-hydrology observation system in a small alpine watershed in the Qilian
759 Mountains of China and its meteorological gradient. Arct. Antarct. Alp. Res. 46 (2),
760 505-523.
761 Chen, R.S., Yang, Y., Han, C., Liu, J., Kang, E., Song, Y., Liu, Z., 2014b. Field
762 experimental research on hydrological function over several typical underlying
763 surfaces in the cold regions of Western China. Adv. Earth Sci. 29 (4), 507-514 (in
764 chinese).
765 Chen, Y.N., Li, W.H., Deng, H.J., Fang, G.H., Li, Z., 2016. Changes in Central Asia's
766 Water Tower: Past, Present and Future. Sci. Rep. 6 (35458).
767 Cheng, G.D., Li, X., Zhao, W., Xu, Z., Feng, Q., Xiao, S., Xiao, H., 2014. Integrated
768 study of the water–ecosystem–economy in the Heihe River Basin. Natl. Sci. Rev. 1
769 (3), 413-428.
770 Clark, M.P., Bierkens, M.F., Samaniego, L., Woods, R.A., Uijlenhoet, R., Bennett, K.E.,
771 Pauwels, V., Cai, X., Wood, A.W., Peters-Lidard, C.D., 2017. The evolution of

772 process-based hydrologic models: historical challenges and the collective quest for
773 physical realism. Hydrol. Earth Syst. Sci. 21.
774 Cobos, D.R., Chambers, C., 2010. Calibrating ECH2O soil moisture sensors.
775 Application Note. Decagon Devices, Pullman, WA.
776 Della Chiesa, S., Bertoldi, G., Niedrist, G., Obojes, N., Endrizzi, S., Albertson, J.D.,
777 Wohlfahrt, G., Hörtnagl, L., Tappeiner, U., 2014. Modelling changes in grassland
778 hydrological cycling along an elevational gradient in the Alps. Ecohydrology 7 (6),
779 1453-1473.
780 Dorigo, W.A., Wagner, W., Hohensinn, R., Hahn, S., Paulik, C., Xaver, A., Gruber, A.,
781 Drusch, M., Mecklenburg, S., Oevelen, P.V., 2011. The International Soil Moisture
782 Network: a data hosting facility for global in situ soil moisture measurements.
783 Hydrol. Earth Syst. Sci. 15 (5), 1675-1698.
784 Dorigo, W., Xaver, A., Vreugdenhil, M., Gruber, A., Hegyiová, A., Sanchis-Dufau, A.,
785 Zamojski, D., Cordes, C., Wagner, W., Drusch, M.,2013. Global automated quality
786 control of in situ soil moisture data from the International Soil Moisture Network.
787 Vadose Zone J. 12 (3).
788 Famiglietti, J.S., Ryu, D., Berg, A.A., Rodell, M., Jackson, T.J., 2008. Field
789 observations of soil moisture variability across scales. Water Resour. Res. 44 (1).
790 Farmer, D., Sivapalan, M., Jothityangkoon, C., 2003. Climate, soil, and vegetation
791 controls upon the variability of water balance in temperate and semiarid landscapes:
792 Downward approach to water balance analysis. Water Resour. Res. 39 (2).
793 Farrick, K.K., Branfireun, B.A., 2014. Soil water storage, rainfall and runoff
794 relationships in a tropical dry forest catchment. Water Resour. Res. 50 (12), 9236-
795 9250.
796 Feddes, R.A., Kowalik, P.J., Zaradny, H., 1978. Simulation of field water use and crop
797 yield. Wageningen : Centre for agricultural publishing and documentation.

798 Feng, Q., Su, Y.H., Si, J.H., Chang, Z.Q., H, X., Guo, R., Chen, L.J., Huo, H., Qin, Y.Y.,
799 2013. Ecohydrological Transect Survey of Heihe River Basin. Adv. Earth Sci. 28
800 (2), 10.
801 Gasch, C., Brown, D., Campbell, C., Cobos, D., Brooks, E., Chahal, M., Poggio, M.,
802 2017. A Field‐Scale Sensor Network Data Set for Monitoring and Modeling the
803 Spatial and Temporal Variation of Soil Water Content in a Dryland Agricultural
804 Field. Water Resour. Res. 53 (12), 10878-10887.
805 Germann, P., Hensel, D., 2006. Poiseuille flow geometry inferred from velocities of
806 wetting fronts in soils. Vadose Zone J. 5 (3), 867-876.
807 Graham, C.B., Lin, H.S., 2011. Controls and frequency of preferential flow occurrence:
808 A 175-event analysis. Vadose Zone J. 10 (3), 816-831.
809 Green, T.R., Erskine, R.H., 2011. Measurement and inference of profile soil‐water
810 dynamics at different hillslope positions in a semiarid agricultural watershed. Water
811 Resour. Res. 47 (12).
812 Guo, L., Lin, H., 2018. Chapter Two - Addressing Two Bottlenecks to Advance the
813 Understanding of Preferential Flow in Soils. In: D.L. Sparks (Editor), Advances in
814 Agronomy. Academic Press, 61-117.
815 Hardie, M., Lisson, S., Doyle, R., Cotching, W., 2013. Determining the frequency, depth
816 and velocity of preferential flow by high frequency soil moisture monitoring. J.
817 Contam. Hydrol. 144 (1), 66-77.
818 He, C.S., Demarchi, C., Ⅱ, T.E.C., Feng, Q., Hunter, T., 2009. Hydrologic modeling
819 of the Heihe watershed by DLBRM in Northwest China. Sci. Cold Arid. Reg. 1 (5),
820 432-442.
821 He, L., Ivanov, V.Y., Bohrer, G., Thomsen, J.E., Vogel, C.S., Moghaddam, M., 2013.
822 Temporal dynamics of soil moisture in a northern temperate mixed successional
823 forest after a prescribed intermediate disturbance. Agric. For. Meteorol. 180 (19),
824 22–33.

825 He, Z.B., Zhao, W.Z., Liu, H., Chang, X.X., 2012. The response of soil moisture to
826 rainfall event size in subalpine grassland and meadows in a semi-arid mountain
827 range: A case study in northwestern China's Qilian Mountains. J. Hydrol. 420–421,
828 183-190.
829 Hoffman, G.J., Van Genuchten, M.T., 1983. Soil properties and efficient water use:
830 Water namagement for salinity control, in: Limitations and Efficient Water Use in
831 Crop Production. American Society Of Agrononmy, Madison, WI, 73-85.
832 Immerzeel, W.W., Van Beek, L.P., Bierkens, M.F., 2010. Climate change will affect the
833 Asian water towers. Science 328 (5984), 1382-1385.
834 Jenny, H., 1994. Factors of soil formation: a system of quantitative pedology. Courier
835 Corporation, Massachusetts, USA.
836 Jian, S.Q., Zhao, C.Y., Fang, S.M., Yu, K., 2015. Effects of different vegetation
837 restoration on soil water storage and water balance in the Chinese Loess Plateau.
838 Agric. For. Meteorol. 206, 85-96.
839 Jin, X., Zhang, L., Gu, J., Zhao, C., Tian, J., He, C., 2015. Modelling the impacts of
840 spatial heterogeneity in soil hydraulic properties on hydrological process in the
841 upper reach of the Heihe River in the Qilian Mountains, Northwest China. Hydrol.
842 Process. 29 (15), 3318-3327.
843 Jin, Z., Guo, L., Lin, H., Wang, Y., Yu, Y., Chu, G., Zhang, J., et al., 2018. Soil moisture
844 response to rainfall on the Chinese Loess Plateau after a long-term vegetation
845 rehabilitation. Hydrol. Process. 32 (12), 1738-1754.
846 Jung, M. et al., 2010. Recent decline in the global land evapotranspiration trend due to
847 limited moisture supply. Nature 467, 951.
848 Kim, S., 2009. Characterization of soil moisture responses on a hillslope to sequential
849 rainfall events during late autumn and spring. Water Resour. Res. 45 (9).
850 Koster, R.D., Dirmeyer, P.A., Zhichang, G., Gordon, B., Edmond, C., Peter, C., Gordon,
851 C.T., Shinjiro, K., Eva, K., David, L., 2004. Regions of strong coupling between
852 soil moisture and precipitation. Science 305 (5687), 1138-1140.

853 Krzywinski, M., Altman, N., 2014. Points of significance: visualizing samples with box
854 plots. Nature Publishing Group, London, UK.
855 Kurc, S.A., Small, E.E., 2004. Dynamics of evapotranspiration in semiarid grassland
856 and shrubland ecosystems during the summer monsoon season, central New
857 Mexico. Water Resour Res. 40 (9).
858 Laio, F., Porporato, A., Ridolfi, L., Rodriguez-Iturbe, I., 2001. Plants in water-
859 controlled ecosystems: active role in hydrologic processes and response to water
860 stress : II. Probabilistic soil moisture dynamics. Adv. Water Resour. 24 (7), 695-
861 705.
862 Li, N., Wang, X.J., Shi, M.J., Yang, H., 2015a. Economic Impacts of Total Water Use
863 Control in the Heihe River Basin in Northwestern China—An Integrated CGE-
864 BEM Modeling Approach. Sustainability 7 (3), 3460-3478.
865 Li, Q., Zhu, Q., Zheng, J., Liao, K., Yang, G., 2015b. Soil Moisture Response to Rainfall
866 in Forestland and Vegetable Plot in Taihu Lake Basin,China. Chin. Geog. Sci. 25
867 (4), 426-437.
868 Li, X., Cheng, G., Liu, S., Xiao, Q., Ma, M., Jin, R., Che, T., Liu, Q., Wang, W., Qi, Y.,
869 2013b. Heihe watershed allied telemetry experimental research (HiWATER):
870 Scientific objectives and experimental design. Bull. Am. Meteorol. Soc. 94 (8),
871 1145-1160.
872 Li, X.Y., Yang, D.W., Zheng, C.M., Li, X.R., Zhao, W.Z., Huang, M.B., Chen, Y.N., Yu,
873 P.T., 2017. Ecohydrology, The Geographical Sciences During 1986—2015: From
874 the Classics To the Frontiers. Springer Singapore, Singapore, pp. 407-417.
875 Li, X.Y., Yang, X.F., Ma, Y.J., Hu, G.R., Hu, X., Wu, X.C., Wang, P., Huang, Y.M., Cui,
876 B.L., Wei, J.Q., 2018. Qinghai Lake Basin Critical Zone Observatory on the
877 Qinghai-Tibet Plateau. Vadose Zone J. 17 (1).
878 Li, X.Y., Zhang, S.Y., Peng, H.Y., Xia, H., Ma, Y.J., 2013a. Soil water and temperature
879 dynamics in shrub-encroached grasslands and climatic implications: Results from

Inner Mongolia steppe ecosystem of north China. Agric. For. Meteorol. 171 (8), 20–30.

Li, Z., Xu, Z., Shao, Q., Yang, J., 2009. Parameter estimation and uncertainty analysis of SWAT model in upper reaches of the Heihe river basin. Hydrol. Process. 23 (19), 2744-2753.

Liang, W.L., Kosugi, K.I., Mizuyama, T., 2011. Soil water dynamics around a tree on a hillslope with or without rainwater supplied by stemflow. Water Resour. Res. 47 (2), 2144-2150.

Lin, H., Zhou, X., 2008. Evidence of subsurface preferential flow using soil hydrologic monitoring in the Shale Hills catchment. Eur. J. Soil Sci. 59 (1), 34–49.

Liniger, H., Weingartner, R., Grosjean, M., 1998. Mountains of the World: Water Towers for the 21st Century. University of Berne, Berne, Switzerland.

Liu, H., Zhao, W., He, Z., Liu, J., 2015. Soil moisture dynamics across landscape types in an arid inland river basin of Northwest China. Hydrol. Process. 3328-3341.

Liu, Y.Y., Peng, H.H., Meng, W.P., Bie, Q., Wang, Y., Zhao, C.Y., 2013. Artificial rainfall interception characteristics in alpine meadows under diferent grazing scenarios in the upper reach of Heihe River. J. Lanzhou Univ. Nat. Sci. 49 (6), 799-806 (in Chinese).

Liu, Z.W., Chen, R.S., Song, Y.X., Han, C.T., 2012. Characteristics of rainfall interception for four typical shrubs in Qilian Mountain. Acta Ecol. Sin. 32 (4), 1337-1346 (in Chinese).

Lozano-Parra, J., Schaik, N.L.M.B.V., Schnabel, S., Gómez-Gutiérrez, Á., 2016. Soil moisture dynamics at high temporal resolution in a semiarid mediterranean watershed with scattered tree cover. Hydrol. Process. 30 (8), 1155-1170.

Lozano-Parra, J., Schnabel, S., Ceballos-Barbancho, A., 2015. The role of vegetation covers on soil wetting processes at rainfall event scale in scattered tree woodland of Mediterranean climate. J. Hydrol. 529, 951-961.

907 Lutz, A.F., Immerzeel, W.W., Shrestha, A.B., Bierkens, M.F.P., 2014. Consistent
908 increase in High Asia's runoff due to increasing glacier melt and precipitation. Nat.
909 Clim. Change 4, 587-592.
910 McColl, K.A., Alemohammad, S.H., Akbar, R., Konings, A.G., Yueh, S., Entekhabi, D.,
911 2017. The global distribution and dynamics of surface soil moisture. Nat. Geosci.
912 10 (2), 100-104.
913 McDonnell, J.J., Beven, K., 2014. Debates—The future of hydrological sciences: A
914 (common) path forward? A call to action aimed at understanding velocities,
915 celerities and residence time distributions of the headwater hydrograph. Water
916 Resour. Res. 50 (6), 5342-5350.
917 McGill, R., Tukey, J.W., Larsen, W.A., 1978. Variations of Box Plots. Am. Stat. 32 (1),
918 12-16.
919 McKenzie, N., Coughlan, K., Cresswell, H., 2002. Soil physical measurement and
920 interpretation for land evaluation, 5. Csiro Publishing, Victoria, Australia.
921 McMillan, H.K., Srinivasan, M.S., 2015. Characteristics and controls of variability in
922 soil moisture and groundwater in a headwater catchment. Hydrol. Earth Syst. Sci.
923 19 (4), 1767-1786.
924 Moran, M.S. et al., 2010. Hydrologic response to precipitation pulses under and
925 between shrubs in the Chihuahuan Desert, Arizona. Water Resour. Res. 46 (10).
926 Muenchen, R.A., 2011. R for SAS and SPSS users. Springer Science & Business Media,
927 Germany.
928 Ochsner, T.E. et al., 2013. State of the Art in Large-Scale Soil Moisture Monitoring.
929 Soil Sci. Soc. Am. J. 77 (6), 1888-1919.
930 Pan, Q.M., Tian, S.L., 2001. Water resources in the Heihe river basin. The Yellow River
931 Water Conservency Press, Zheng Zhou, China.
932 Pan, X.D., Li, X., Yang, K., He, J., Zhang, Y., Han, X., 2014. Comparison of
933 downscaled precipitation data over a mountainous watershed: A case study in the
934 Heihe River Basin. J. Hydrometeorol. 15 (4), 1560-1574.

935 Pellet, C., Hauck, C., 2017. Monitoring soil moisture from middle to high elevation in
936 Switzerland: set-up and first results from the SOMOMOUNT network. Hydrol.
937 Earth Syst. Sci. 21 (6), 3199-3220.
938 Quiring, S.M., Ford, T.W., Wang, J.K., Khong, A., Harris, E., Lindgren, T., Goldberg,
939 D.W., Li, Z., 2016. The North American Soil Moisture Database: Development and
940 Applications. Bull. Am. Meteorol. Soc. 97 (8), 1441-1459.
941 Ran, Y.H., Li, X., Cheng, G.D., 2018. Climate warming over the past half century has
942 led to thermal degradation of permafrost on the Qinghai-Tibet Plateau. Cryosphere
943 12 (2), 595-608.
944 Reatto, A., da Silva, E.M., Bruand, A., Martins, E.S., Lima, J.E.F.W., 2008. Validity of
945 the centrifuge method for determining the water retention properties of tropical
946 soils. Soil Sci. Soc. Am. J. 72 (6), 1547-1553.
947 Rosenbaum, U., Bogena, H., Herbst, M., Huisman, J., Peterson, T., Weuthen, A.,
948 Western, A., Vereecken, H., 2012. Seasonal and event dynamics of spatial soil
949 moisture patterns at the small catchment scale. Water Resour. Res. 48 (10).
950 Rossi, M.J., Ares, J.O., Jobbágy, E.G., Vivoni, E.R., Vervoort, R.W., Schreiner-McGraw,
951 A.P., Saco, P.M., 2018. Vegetation and terrain drivers of infiltration depth along a
952 semiarid hillslope. Sci. Total Environ. 644, 1399-1408.
953 Saito, T., Fujimaki, H., Yasuda, H., Inosako, K., Inoue, M., 2013. Calibration of
954 Temperature Effect on Dielectric Probes Using Time Series Field Data. Vadose
955 Zone J. 12 (2).
956 Saito, T., Fujimaki, H., Yasuda, H., Inoue, M., 2009. Empirical Temperature Calibration
957 of Capacitance Probes to Measure Soil Water. Soil Sci. Soc. Am. J. 73 (6), 1931-
958 1937.
959 Seneviratne, S.I., Corti, T., Davin, E.L., Hirschi, M., Jaeger, E.B., Lehner, I., Orlowsky,
960 B., Teuling, A.J., 2010. Investigating soil moisture–climate interactions in a
961 changing climate: a review. Earth Sci. Rev. 99 (3), 125-161.

962 Shi, Y.N., Baldwin, D.C., Davis, K.J., Yu, X., Duffy, C.J., Lin, H., 2015. Simulating
963 high-resolution soil moisture patterns in the Shale Hills watershed using a land
964 surface hydrologic model. Hydrol. Process. 29 (21), 4624-4637.
965 Simunek, J., Van Genuchten, M.T., Sejna, M., 2005. The HYDRUS-1D software
966 package for simulating the one-dimensional movement of water, heat, and multiple
967 solutes in variably-saturated media. Univ. Calif. - Riverside Res. Rep. 3, 1-240.
968 Su, Z., Wen, J., Dente, L., van der Velde, R., Wang, L., Ma, Y., Yang, K., Hu, Z., 2011.
969 The Tibetan Plateau observatory of plateau scale soil moisture and soil temperature
970 (Tibet-Obs) for quantifying uncertainties in coarse resolution satellite and model
971 products. Hydrol. Earth Syst. Sci. 15 (7), 2303-2316.
972 Sun, F.X., Lü, Y.H., Wang, J.L., Hu, J., Fu, B.J., 2015. Soil moisture dynamics of typical
973 ecosystems in response to precipitation: A monitoring-based analysis of
974 hydrological service in the Qilian Mountains. Catena 129 (1), 63-75.
975 Thompson, S.E., Harman, C.J., Troch, P.A., Brooks, P.D., Sivapalan, M., 2011. Spatial
976 scale dependence of ecohydrologically mediated water balance partitioning: A
977 synthesis framework for catchment ecohydrology. Water Resour. Res. 47 (10).
978 Tian, J., Zhang, B.Q., He, C.S., Yang, L.X., 2017. Variability in Soil Hydraulic
979 Conductivity and Soil Hydrological Response Under Different Land Covers in the
980 Mountainous Area of the Heihe River Watershed, Northwest China. Land Degrad.
981 Dev. 28 (4), 1437-1449.
982 Van Genuchten, M.T., 1980. A closed-form equation for predicting the hydraulic
983 conductivity of unsaturated soils. Soil Sci. Soc. Am. J. 44 (5), 892-898.
984 Vereecken, H., Huisman, J.A., Franssen, H.J.H., Brüggemann, N., Bogena, H.R., Kollet,
985 S., Javaux, M., Kruk, J.V.D., Vanderborght, J., 2015. Soil hydrology: Recent
986 methodological advances, challenges, and perspectives. Water Resour. Res. 51 (4),
987 2616-2633.

988 Viviroli, D. et al., 2011. Climate change and mountain water resources: overview and
989 recommendations for research, management and policy. Hydrol. Earth Syst. Sci. 15
990 (2), 471-504.
991 Wang, G.X., Liu, G.S., Li, C.J., Yang, Y., 2012b. The variability of soil thermal and
992 hydrological dynamics with vegetation cover in a permafrost region. Agric. For.
993 Meteorol. 162–163, 44-57.
994 Wang, G.X., Wang, Y.B., Li, Y.S., Cheng, H.Y., 2007. Influences of alpine ecosystem
995 responses to climatic change on soil properties on the Qinghai–Tibet Plateau, China.
996 Catena 70 (3), 506-514.
997 Wang, H.L., Tetzlaff, D., Soulsby, C., 2018. Modelling the effects of land cover and
998 climate change on soil water partitioning in a boreal headwater catchment. J.
999 Hydrol. 558, 520-531.
1000 Wang, Q.F., Jin, H., Zhang, T., Cao, B., Peng, X., Wang, K., Xiao, X., Guo, H., Mu, C.,
1001 Li, L., 2017. Hydro-thermal processes and thermal offsets of peat soils in the active
1002 layer in an alpine permafrost region, NE Qinghai-Tibet plateau. Global Planet.
1003 Change 156, 1-12.
1004 Wang, S., Fu, B., Gao, G., Zhou, J., Jiao, L., Liu, J., 2015. Linking the soil moisture
1005 distribution pattern to dynamic processes along slope transects in the Loess Plateau,
1006 China. Environ. Monit. Assess. 187 (12).
1007 Wang, S., Fu, B.J., Gao, G.Y., Liu, Y., Zhou, J., 2013. Responses of soil moisture in
1008 different land cover types to rainfall events in a re-vegetation catchment area of the
1009 Loess Plateau, China. Catena 101, 122-128.
1010 Wang, S., Fu, B.J., Gao, G.Y., Yao, X.L., Zhou, J., 2012a. Soil moisture and
1011 evapotranspiration of different land cover types in the Loess Plateau, China. Hydrol.
1012 Earth Syst. Sci. 16 (8), 2883-2892.
1013 Wang, X.P., Cui, Y., Pan, Y.-X., Li, X.R., Yu, Z., Young, M.H., 2008. Effects of rainfall
1014 characteristics on infiltration and redistribution patterns in revegetation-stabilized
1015 desert ecosystems. J. Hydrol. 358 (1), 134-143.

1016 Western, A.W., Zhou, S.L., Grayson, R.B., McMahon, T.A., Blöschl, G., Wilson, D.J.,
1017 2004. Spatial correlation of soil moisture in small catchments and its relationship
1018 to dominant spatial hydrological processes. J. Hydrol. 286 (1), 113-134.
1019 Wiekenkamp, I., Huisman, J.A., Bogena, H.R., Lin, H.S., Vereecken, H., 2016. Spatial
1020 and temporal occurrence of preferential flow in a forested headwater catchment. J.
1021 Hydrol. 534, 139-149.
1022 Xiong, Z., Yan, X., 2013. Building a high-resolution regional climate model for the
1023 Heihe River Basin and simulating precipitation over this region. Chin. Sci. Bull. 58
1024 (36), 4670-4678.
1025 Yang, D.W., Gao, B., Jiao, Y., Lei, H., Zhang, Y., Yang, H., Cong, Z., 2015. A distributed
1026 scheme developed for eco-hydrological modeling in the upper Heihe River. Sci.
1027 China: Earth Sci. 58 (1), 36-45.
1028 Yang, J.J., He, Z.B., Du, J., Chen, L.F., Zhu, X., Lin, P.F., Li, J., 2017. Soil water
1029 variability as a function of precipitation, temperature, and vegetation: a case study
1030 in the semiarid mountain region of China. Environ. Earth Sci. 76 (5), 206.
1031 Yang, K., Qin, J., Zhao, L., Chen, Y., Tang, W., Han, M., Chen, Z., Lv, N., Ding, B.,
1032 Wu, H., 2013. A multiscale soil moisture and freeze-thaw monitoring network on
1033 the third pole. Bull. Am. Meteorol. Soc. 94 (12), 1907-1916.
1034 Yao, Y.Y., Zheng, C., Andrews, C., Zheng, Y., Zhang, A., Liu, J., 2017. What Controls
1035 the Partitioning between Baseflow and Mountain Block Recharge in the Qinghai‐
1036 Tibet Plateau? Geophys. Res. Lett. 44 (16), 8352-8358.
1037 Yu, X.N., Huang, Y.M., Li, E.G., Li, X.Y., Guo, W.H., 2017. Effects of vegetation types
1038 on soil water dynamics during vegetation restoration in the Mu Us Sandy Land,
1039 northwestern China. J. Arid Land 9 (2), 188-199.
1040 Yu, Y., Wei, W., Chen, L.D., Jia, F.Y., Yang, L., Zhang, H.D., Feng, T.J., 2015.
1041 Responses of vertical soil moisture to rainfall pulses and land uses in a typical loess
1042 hilly area, China. Solid Earth 6 (2), 595-608.

1043 Zehe, E., Becker, R., Bárdossy, A., Plate, E., 2005. Uncertainty of simulated catchment
1044 runoff response in the presence of threshold processes: Role of initial soil moisture
1045 and precipitation. J. Hydrol. 315 (1), 183-202.
1046 Zeng, C., Zhang, F., Wang, Q.J., Chen, Y.Y., Joswiak, D.R., 2013. Impact of alpine
1047 meadow degradation on soil hydraulic properties over the Qinghai-Tibetan Plateau.
1048 J. Hydrol. 478, 148-156.
1049 Zhang, A.J., Liu, W.B., Yin, Z.L., Fu, G.B., Zheng, C.M., 2016. How Will Climate
1050 Change Affect the Water Availability in the Heihe River Basin, Northwest China?
1051 J. Hydrometeorol. 17 (5), 1517-1542.
1052 Zhang, L.H., He, C.S., Bai, X., Zhu, Y., 2017b. Physically Based Adjustment Factors
1053 for Precipitation Estimation in a Large Arid Mountainous Watershed, Northwest
1054 China. J. Hydrol. Eng. 22 (11), 04017047.
1055 Zhang, L.H., He, C.S., Zhang, M.M., 2017a. Multi-Scale Evaluation of the SMAP
1056 Product Using Sparse In-Situ Network over a High Mountainous Watershed,
1057 Northwest China. Remote Sens. 9 (11), 1111.
1058 Zhang, X.Z., Xiong, Z., Zheng, J.Y., Ge, Q.S., 2018. High-resolution precipitation data
1059 derived from dynamical downscaling using the WRF model for the Heihe River
1060 Basin, northwest China. Theor. Appl. Climatol. 131 (3), 1249-1259.
1061 Zhao, C. et al., 2014. Analysis of the relationships between the spatial variations of soil
1062 moisture and the environmental factors in the upstream of the Heihe River
1063 watershed. J. Lanzhou Univ. Nat. Sci. 50 (3), 338-347 (in chinese).
1064 Zhi, J.J., Zhang, G., Yang, F., Yang, R., Liu, F., Song, X., Zhao, Y., Li, D., 2017.
1065 Predicting mattic epipedons in the northeastern Qinghai-Tibetan Plateau using
1066 Random Forest. Geoderma Regional 10, 1-10.
1067 Zhou, J.H. et al., 2016. Alpine vegetation phenology dynamic over 16years and its
1068 covariation with climate in a semi-arid region of China. Sci. Total Environ. 572,
1069 119-128.

1070 Zhu, Q., Nie, X., Zhou, X., Liao, K., Li, H., 2014. Soil moisture response to rainfall at
1071 different topographic positions along a mixed land-use hillslope. Catena 119, 61-
1072 70.
1073

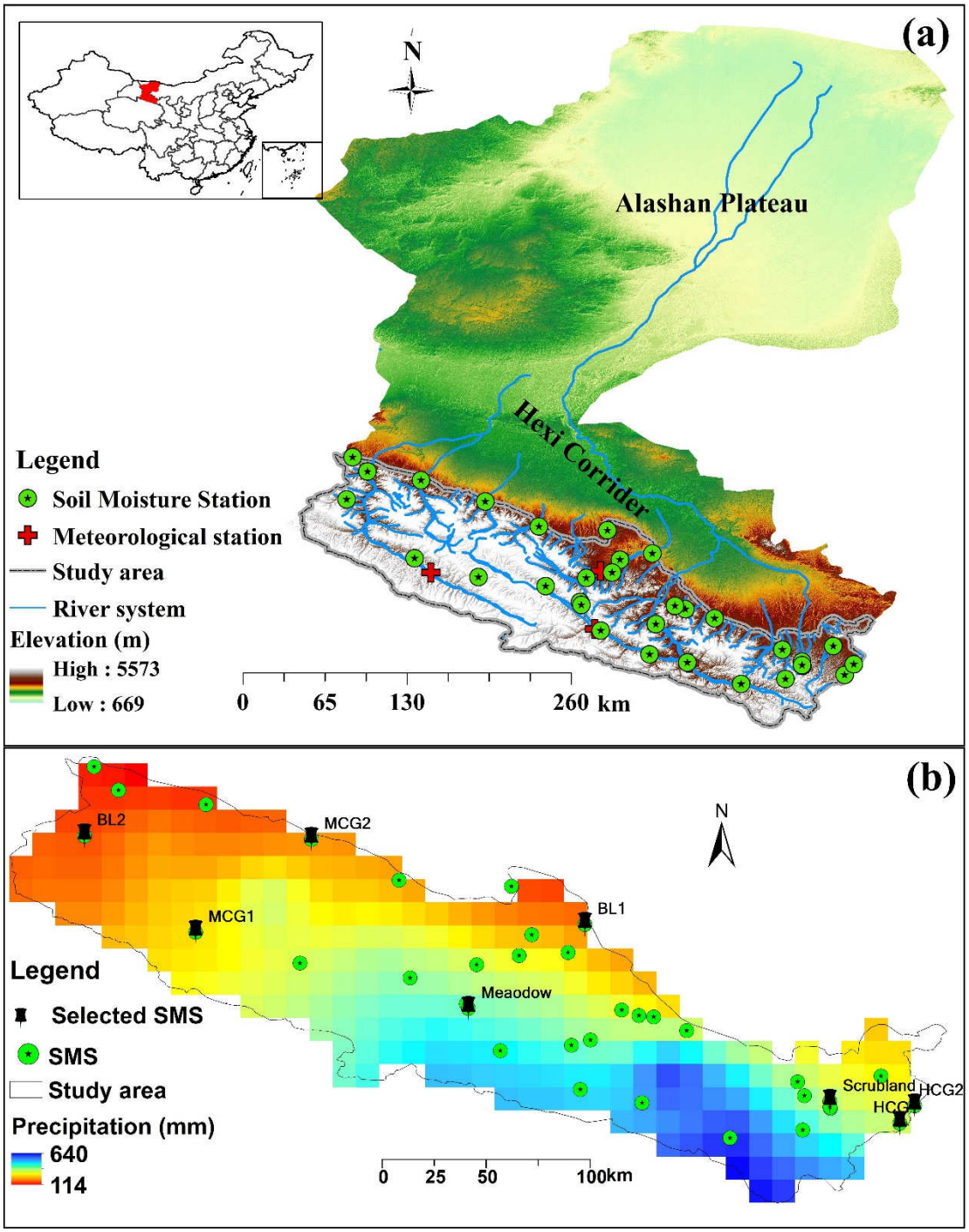

Fig. 1. Location of the study area and the distribution of the soil moisture stations (SMS) (a), and the distribution of the selected SMS in this study, as well as the spatial distribution of the precipitation (annual rainfall of 2014) (b).

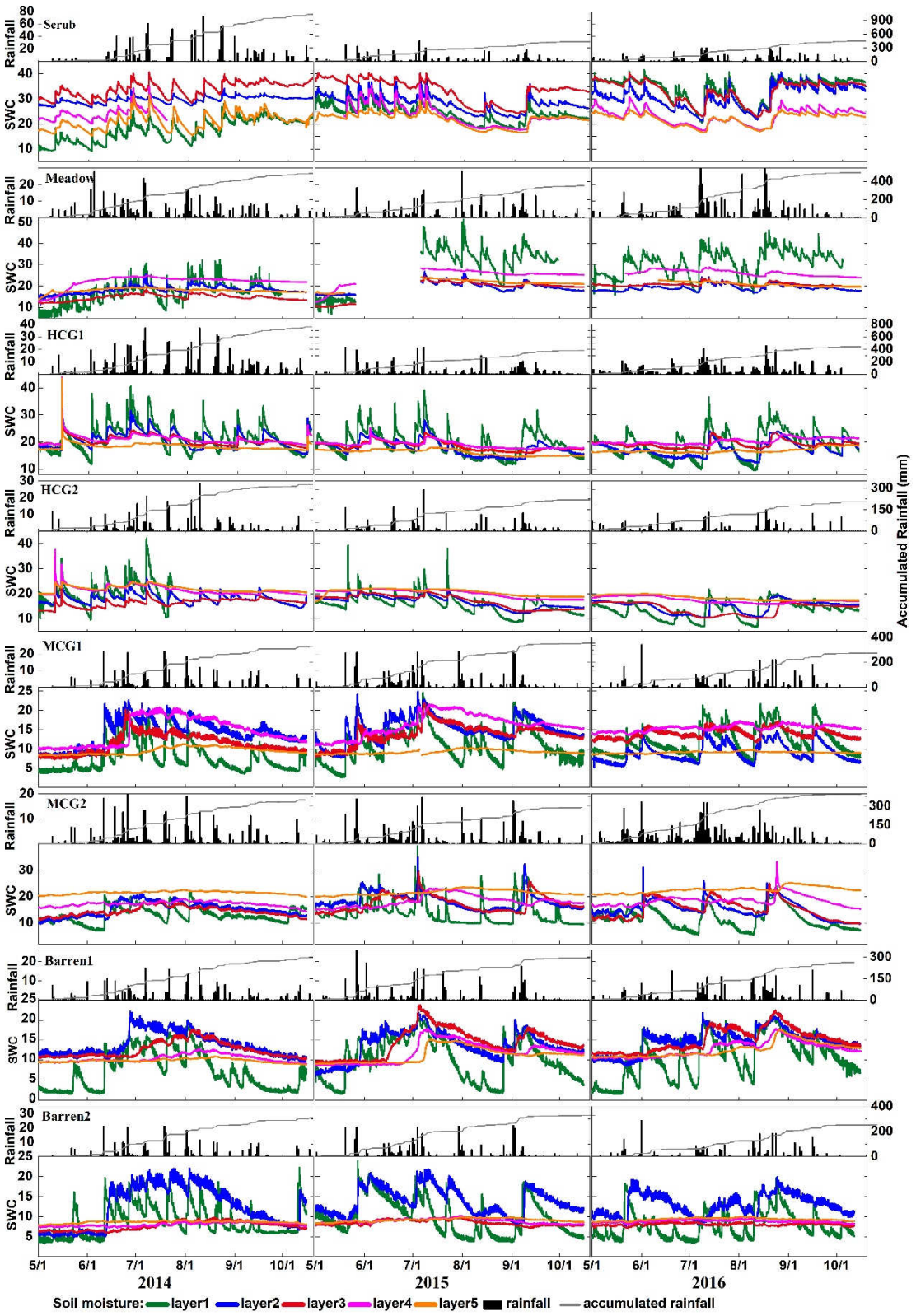

Fig. 2. 0.5 hourly time series of soil moisture (SWC, vol. %) for scrubland (1 soil moisture station: Scrub), meadow (1 station: Meadow), high coverage grassland (2 stations: HCG1, HCG2), medium coverage grassland (2 stations: MCG1, MCG2) and barren land (2 stations: Baren1, Barren2) at soil depths of 5, 15, 25, 40, 60 cm. Gaps exist due to missing data. Also shown are the rainfall data (mm/d) and accumulated rainfall (mm) for each station.

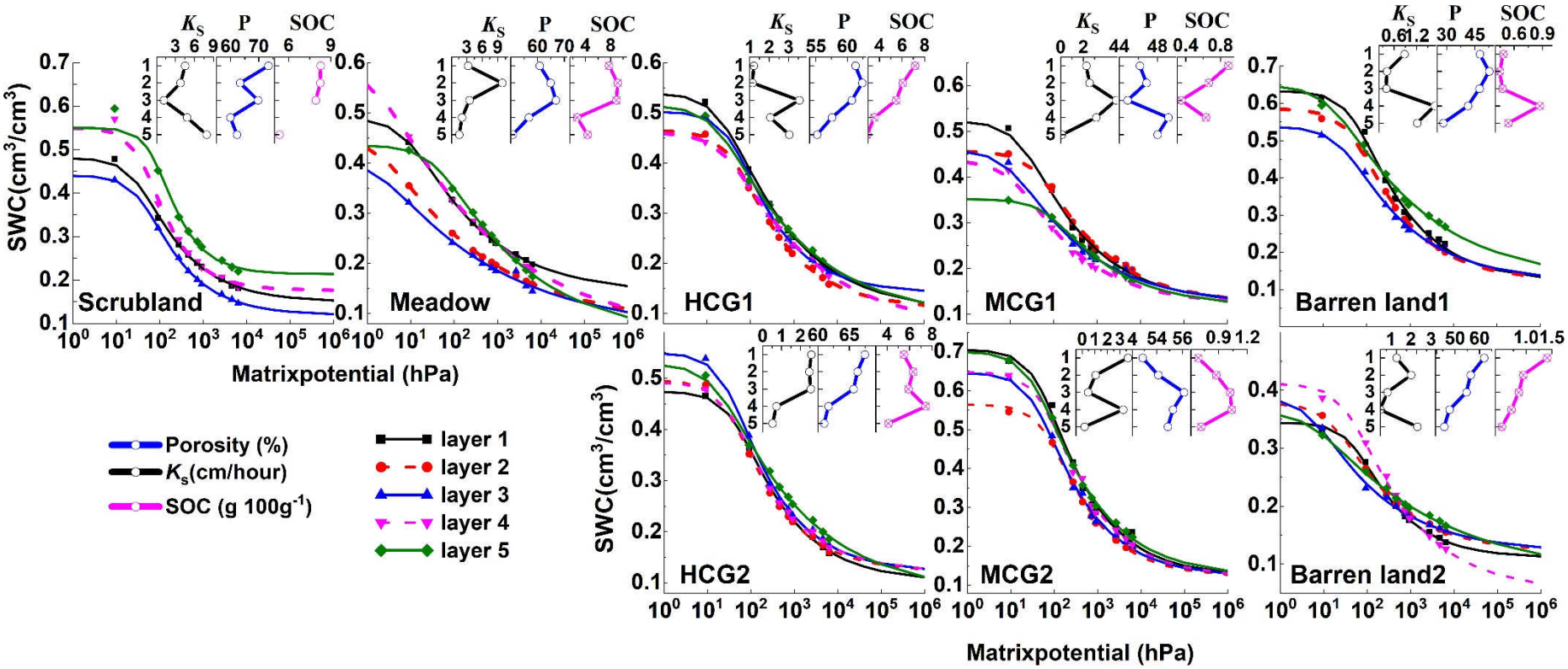

Fig. 3. Profile distribution of the soil retention curve, K_S, soil porosity and SOC of the soil moisture stations. K_S is the saturated hydraulic conductivity (cm/hour), SOC is the soil organic carbon (g $100g^{-1}$), and P is the soil porosity (%)

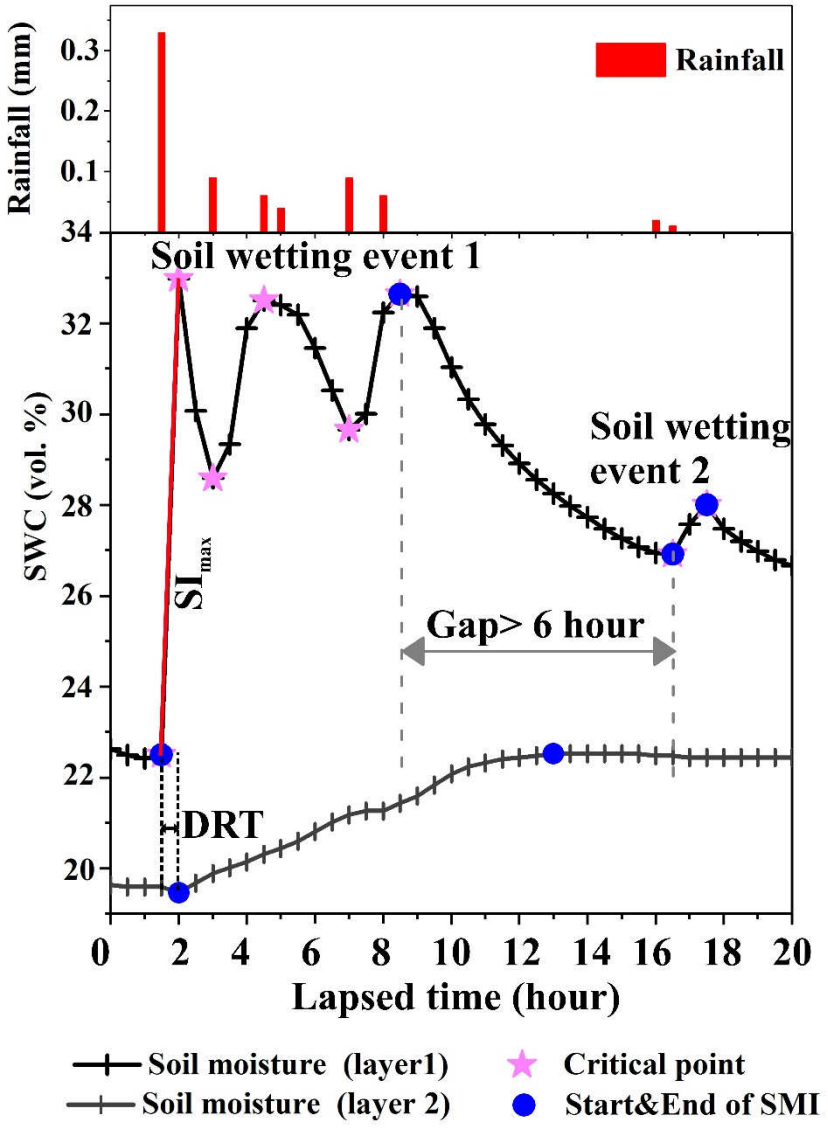

Fig. 4. Example of the identification of soil moisture increment event

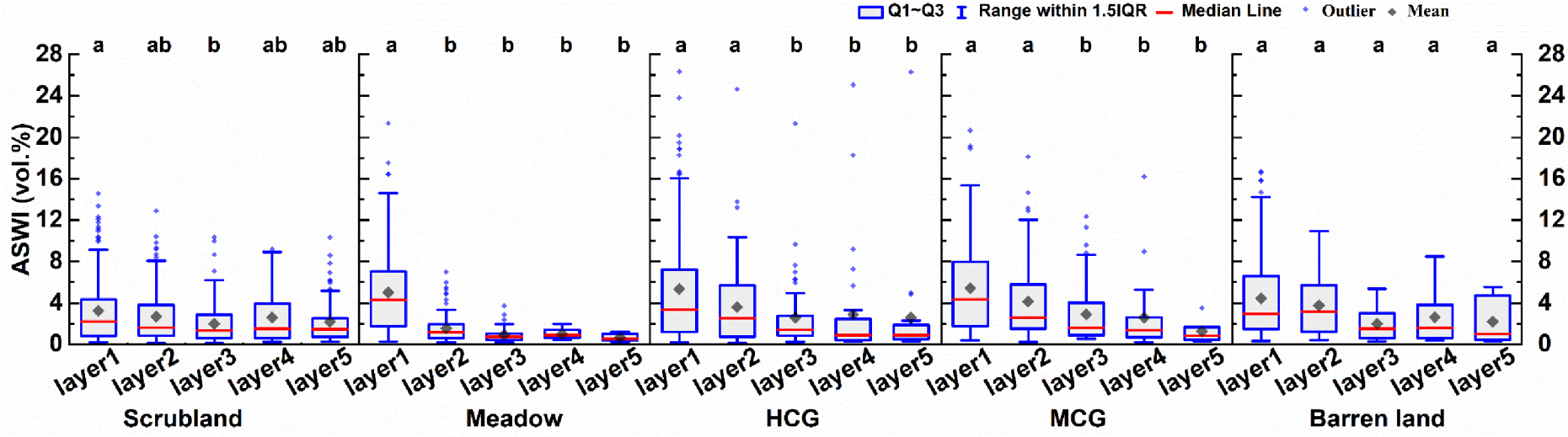

Fig. 5. Profile distribution of ASWI at different layers for different land covers. The different lowercase letters show a significant difference among different soil layers under a specific land cover, and the same letters show the difference of indices among different layers are not significant ($p<0.05$). The range of values in Fig. 5 is different and there are breaks in the axis for graphical purposes to see the variation of SWI with depth for different land covers. Q1 and Q3 are the first and third quartile, IQR is the interquartile range (IQR = Q3−Q1).

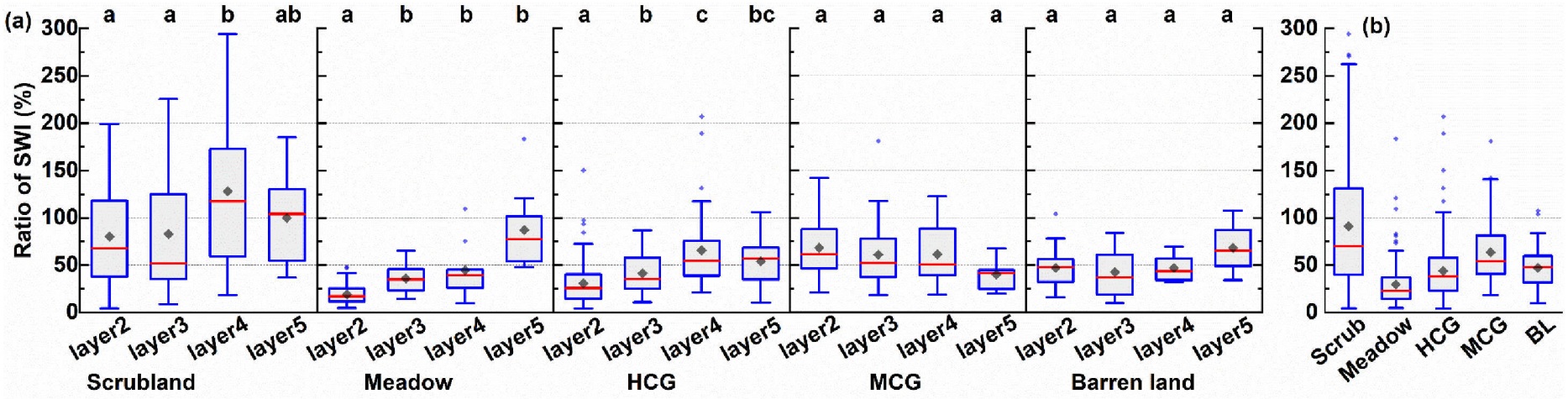

Fig. 6. Profile distribution of Ratio of SWI (RSWI) for different land covers. The different lowercase letters show a significant difference among different soil layers under a specific land covers ($p<0.05$). (b) The result of RSWI of all layers along profile for different land covers.

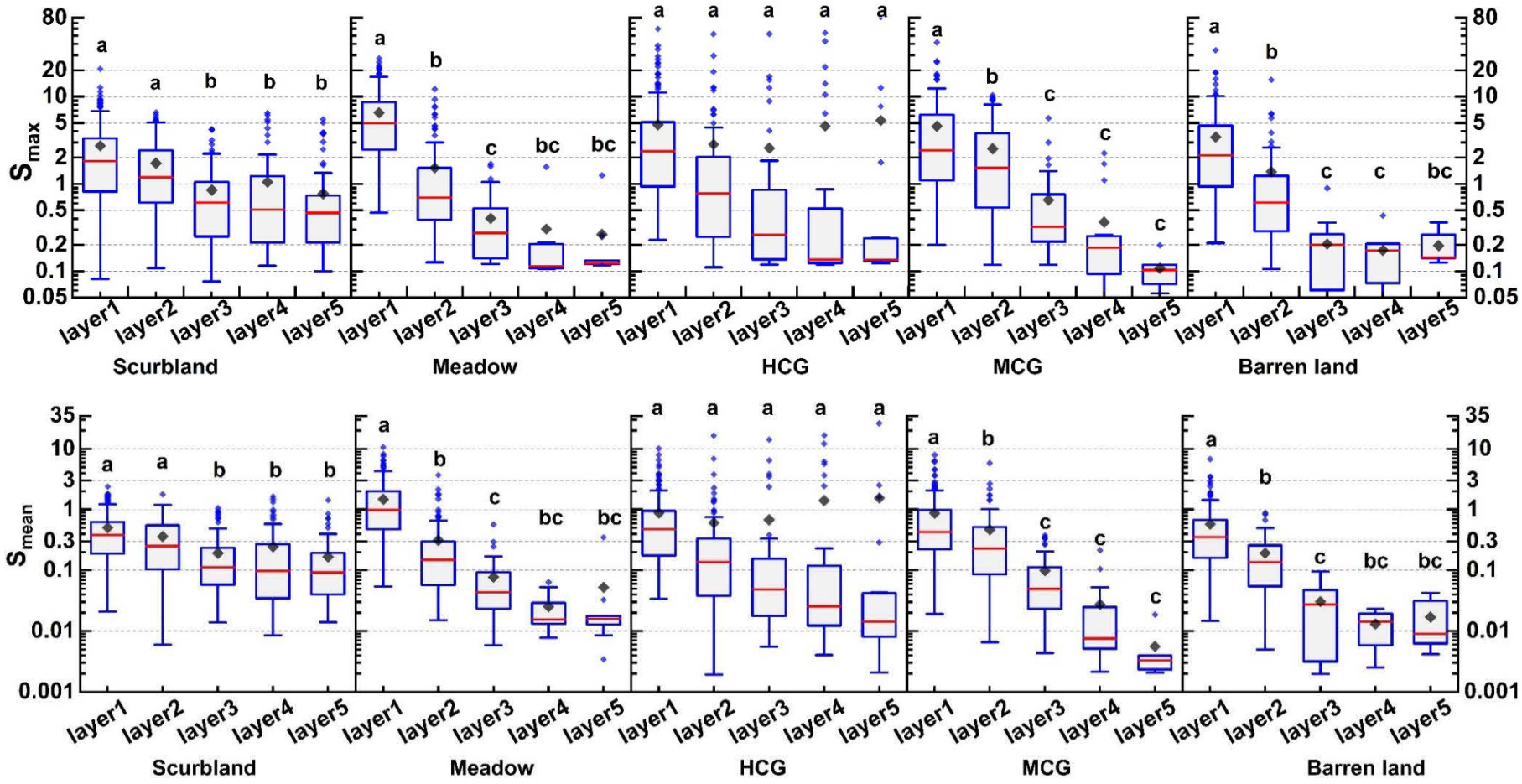

Fig. 7. Profile distribution of S_{max} and S_{mean} for different land covers. S_{max} and S_{mean} are box plotted with lognormal distribution to clearly display the entire distribution of the data. The different lowercase letters in different layers show a significant difference among different soil layers under a specific land cover, and the same lowercase letters in different layers show no significant difference among different layers ($p<0.05$).

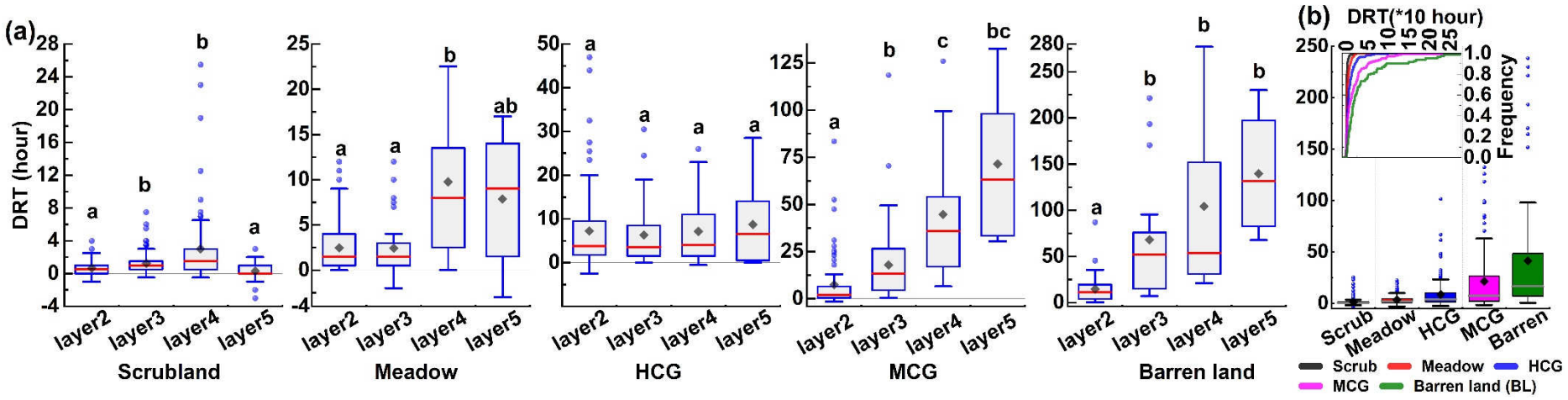

Fig. 8. (a) Profile distribution of different of response time (DRT) under different land covers. The different lowercase letters show a significant difference among different soil layers under a specific land cover ($p<0.05$). (b) The result of the DRT of all layers along profile for different land covers. The inset graph in the right panel shows the accumulated frequency of DRT for different land covers. HCG, MCG and BL is high coverage grassland, medium coverage grassland and barren land, respectively.

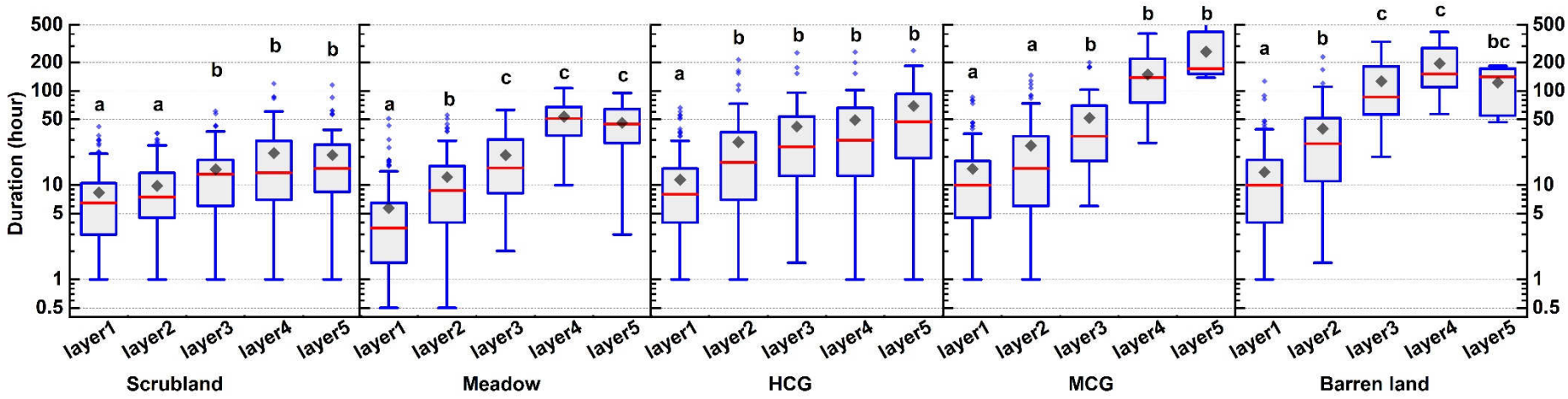

Fig. 9. Profile distribution of duration of the soil wetting events for different land covers. Duration boxes are plotted with lognormal distribution to clearly display the entire distribution of the data. The different lowercase letters show a significant difference among different soil layers under a specific land cover ($p<0.05$).

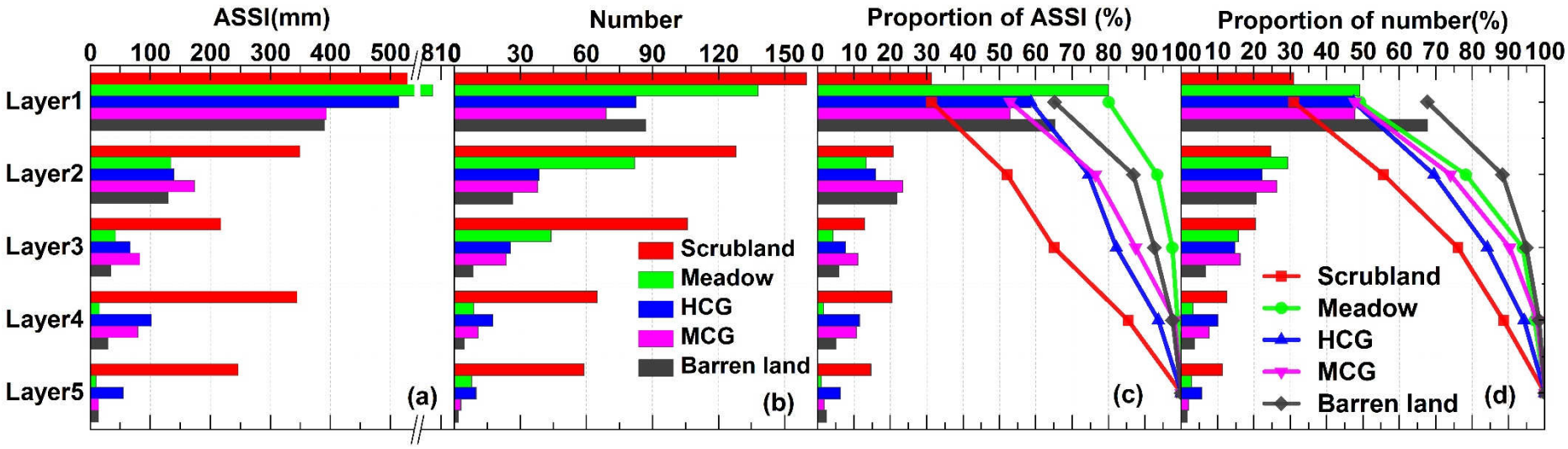

Fig. 10. Profile distribution of (a) accumulated soil storage increment (ASSI, mm) of each layers during the growing season of 2014-2016 under the different land covers. (b) Number of the soil wetting events for different land covers. (c) Proportion of ASSI and the line plot is the vertical variation of the accumulated proportion of ASSI (the colors of the line stand for different land covers, corresponding to the colors of the bar). (d) Proportion of number of the soil wetting events and its accumulated proportion.

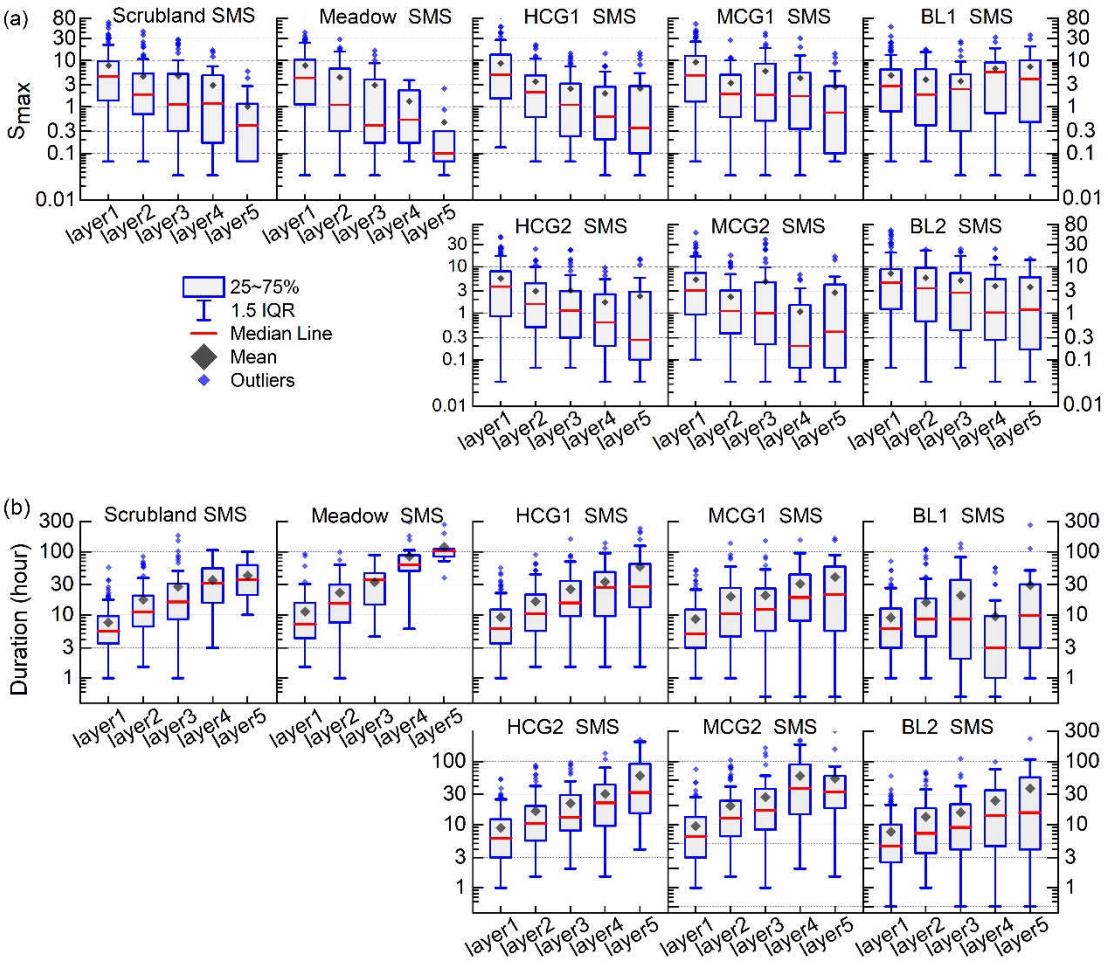

Fig. 11. Box plots of indices of S_{max} (a), and Duration (b) calculated from the simulated soil moisture under the different soil properties with the same plant parameters to test the influence of soil property on the pattern of soil moisture dynamics. X axis is soil layer.

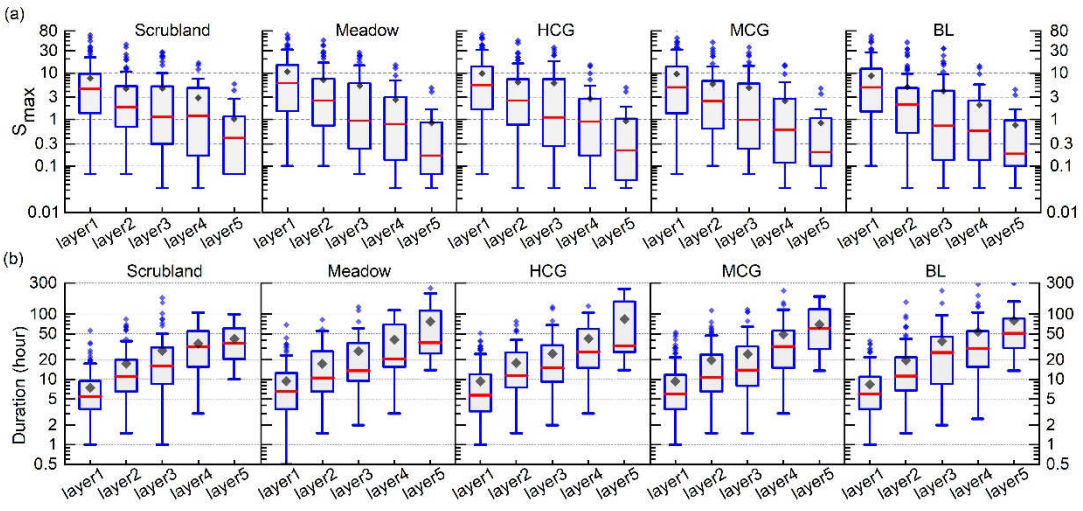

Fig. 12. Box plots of indices of S_{max} (a), and Duration (b) calculated from the simulated soil moisture under the different land covers with the same soil hydraulic properties to test the influence of plant parameters on the pattern of soil moisture dynamics. X axis is soil layer. HCG, MCG and BL represent high coverage grassland, medium coverage grassland and barren land, respectively.

Table 1. Basic characteristics of the selected soil moisture stations.

SMS	Surface-FVC	LAI	Root Depth (cm)	Slope(°)	Aspect(°)	Position	Elevation (m)	Sand(%)	Clay(%)	Silt(%)
Shrub	99%	3.6	>70	0	--	flat	2977	29.021	6.965	64.014
Meadow	100%	3.2	10	8	82	bottom	3800	30.659	7.684	61.656
HCG1	100%	2.6	49	6	65	flat	2558	19.131	4.584	76.285
HCG2	100%	2.5	52	9	257	top	2787	24.928	6.691	68.381
MCG1	35%	0.8	31	0	--	flat	3317	17.203	7.912	74.886
MCG2	30%	0.6	25	8	33	flat	2170	17.474	6.538	75.988
Barren land1	5%	_	_	8	--	mid	1827	24.469	6.184	69.347
Barren land2	8%	_	_	9	197	flat	3117	30.691	6.56	62.749

Note: FVC is the fraction of vegetation coverage, HCG and MCG represent high coverage grassland and medium coverage grassland, respectively. The sand, silt and clay are analyzed according to the United States Department of Agriculture soil classification scheme.

Table 2. The recorded number of soil wetting events at each soil layers of the soil moisture stations.

Layer	scrubland	meadow	HCG1	HCG2	MCG1	MCG2	Barren land1	Barren land2	Sum
layer1	160	155	113	78	87	57	77	95	822
layer2	129	82	41	47	59	24	25	28	435
layer3	110	44	27	24	32	16	6	11	270
layer4	65	9	19	16	15	7	2	7	140
layer5	78	8	12	8	2	4	0	4	116
Sum	542	298	212	173	195	108	110	145	1783

Note: there were gaps in each soil moisture stations, as mentioned in 2.2. HCG and MCG represent high coverage grassland and medium coverage grassland, respectively.

Table 3. The descriptive statistics (Mean±STD) for the indices of specific layers under different land covers.

Index	Shrub	Meadow	HCG	MCG	Barren land
ASWI1	3.3±3.37	5.2±4.22	5.39±5.36	5.01±3.79	4.54±3.86
ASWI2	2.72±2.65	1.64±1.48	3.61±3.81	4.33±3.58	4.91±3.17
ASWI3	2±1.99	0.95±0.71	2.62±3.45	3.43±2.93	4.07±3.59
ASWI4	2.65±2.72	0.86±0.54	2.9±5.16	3.61±3.38	3.35±2.58
ASWI5	2.31±2.19	0.61±0.29	2.75±5.71	2.32±1.04	3.56±2.33
RSWI2	80.28±49.47	19.08±9.93	30.72±23.52	68.26±31.27	46.78±16.77
RSWI3	83.02±75.37	35.96±13.84	41.21±21.2	60.91±33.54	42.39±25.17
RSWI4	127.93±85.65	44.49±30.75	65.74±41.29	61.49±32.55	49.7±13.39
RSWI5	99.9±40.03	87.16±45.36	53.92±25.63	39.79±16.93	67.87±30.25
$S_{max}1$	2.73±2.91	6.6±5.61	4.78±7.37	3.99±5.08	3.47±4.01
$S_{max}2$	1.72±1.5	1.62±2.27	2.82±6.87	2.48±2.6	1.67±2.36
$S_{max}3$	0.85±0.86	0.42±0.37	2.53±8.03	0.77±0.83	0.37±0.14
$S_{max}4$	1.06±1.49	0.31±0.48	4.47±12	0.45±0.53	0.2±0.1
$S_{max}5$	0.81±1.09	0.28±0.4	5.33±18.31	0.13±0.02	0.22±0.08
$S_{mean}1$	0.93±0.79	2.64±2.51	1.6±2.19	1.33±2.27	1.15±1.25
$S_{mean}2$	0.68±0.52	0.63±0.73	1.07±3.2	0.91±1.22	0.6±0.48
$S_{mean}3$	0.36±0.35	0.22±0.15	1.2±3.74	0.33±0.19	0.18±0.02
$S_{mean}4$	0.45±0.55	0.13±0.04	2.27±5.96	0.2±0.11	0.15±0.01
$S_{mean}5$	0.34±0.37	0.18±0.16	1.93±6.51	0.13±0.02	0.15±0.01
DRT2	0.66±0.77	2.49±2.65	7.24±9.37	7.4±14.33	14.61±14.83
DRT3	1.25±1.37	2.42±2.74	6.33±6.84	18±20.58	68.24±67.28
DRT4	3.01±5	9.78±7.77	7.17±7.59	44.64±34.09	104.28±96.6
DRT5	0.3±1.15	7.88±7.52	8.71±9.09	71.5±43.65	140±72.39
Duration1	8.79±7.93	7.79±10.9	18.69±31.03	16.29±18.14	26.08±47.2
Duration2	10.1±8.24	12.38±12.61	35.62±50.75	29.97±42.32	63.52±79.5
Duration3	14.57±11.83	19.25±14.9	58.03±89.35	49.67±46.17	202.86±159.71
Duration4	21.18±19.93	46.06±23.48	64.76±98.54	184.53±119.69	309.81±217.06
Duration5	21.96±19.8	34.57±23.15	88.45±119.44	313.75±167.12	316.63±90.56

Note: HCG and MCG represent high coverage grassland and medium coverage grassland, respectively. ASWI, RSWI, DRT, S_{max} and S_{mean} represent the indexes of the increment of soil wetting event, ratio of ASWI between adjacent soil layers, difference of the soil moisture response time, maximum and mean slope of the soil wetting curve, respectively. The number of 1, 2, 3, 4 and 5 after specific indices represents layers 1, 2, 3, 4 and 5, respectively. HCG and MCG represent high coverage grassland and medium coverage grassland, respectively.

Appendix:

Table A1. Parameters of profile soil hydraulic properties of the different stations. θ_s and θ_r are the saturated and residual water content (cm^3/cm^3), α (1/cm), n, θ_s and θ_r are empirical coefficients fitted by Mualem-van Genuchten model. K_S (cm/hour) is the saturated hydraulic conductivity. SOC is the soil organic carbon (g $100g^{-1}$).

Station	layer	θ_r	θ_s	α	n	K_S	SOC
scrubland	layer1	0.100	0.527	0.091	1.265	4.529	8.270
	layer2	0.094	0.496	0.070	1.297	3.806	8.250
	layer3	0.089	0.465	0.049	1.330	1.161	7.930
	layer4	0.076	0.550	0.023	1.633	4.857	-
	layer5	0.133	0.548	0.012	1.727	7.927	5.350
meadow	layer1	0.080	0.741	0.203	1.202	3.276	9.434
	layer2	0.079	0.441	0.378	1.193	9.847	12.058
	layer3	0.120	0.518	0.130	1.296	3.538	10.923
	layer4	0.020	0.431	0.137	1.164	2.075	3.828
	layer5	0.024	0.431	0.025	1.193	1.564	4.321
HCG1	layer1	0.100	0.538	0.041	1.284	1.218	7.148
	layer2	0.108	0.464	0.024	1.368	1.149	6.071
	layer3	0.140	0.502	0.025	1.413	3.558	5.494
	layer4	0.065	0.460	0.035	1.231	2.068	3.541
	layer5	0.088	0.514	0.054	1.236	3.042	2.927
HCG2	layer1	0.080	0.475	0.026	1.313	2.586	5.494
	layer2	0.110	0.496	0.033	1.367	2.480	6.322
	layer3	0.110	0.550	0.034	1.362	2.562	5.901
	layer4	0.136	0.490	0.024	1.432	0.735	7.425
	layer5	0.080	0.527	0.053	1.238	0.527	4.136
MCG1	layer1	0.040	0.526	0.079	1.197	2.282	0.891
	layer2	0.050	0.459	0.034	1.200	2.550	0.664
	layer3	0.080	0.461	0.126	1.201	4.905	0.349
	layer4	0.100	0.436	0.088	1.262	3.150	0.633
	layer5	0.070	0.353	0.017	1.211	0.117	-
MCG2	layer1	0.060	0.712	0.027	1.292	3.652	0.687
	layer2	0.090	0.579	0.019	1.339	1.067	0.876
	layer3	0.080	0.649	0.030	1.316	0.466	1.022
	layer4	0.110	0.649	0.016	1.383	3.265	1.039
	layer5	0.150	0.704	0.024	1.396	0.191	0.717

Continue Table A1.

Station	layer	θ_r	θ_s	α	n	*K*s	SOC
	layer1	0.030	0.638	0.026	1.242	0.879	1.411
	layer2	0.050	0.595	0.030	1.252	0.411	0.950
BL1	layer3	0.040	0.541	0.049	1.215	0.397	0.858
	layer4	0.042	0.402	0.407	1.143	1.682	0.716
	layer5	0.050	0.654	0.078	1.188	1.218	0.525
	layer1	0.020	0.385	0.044	1.190	1.011	0.485
	layer2	0.035	0.381	0.091	1.214	1.728	0.449
BL2	layer3	0.037	0.392	0.298	1.193	0.555	0.476
	layer4	0.001	0.421	0.041	1.222	0.205	0.872
	layer5	0.037	0.362	0.179	1.159	2.042	0.539

Notes: HCG1 and HCG2 are the stations of high coverage grassland, MCG1 and MCG2 are the stations of medium coverage grassland, and BL1 and BL2 are the stations of barren land.

Table A2. Crop parameters of different land covers for the simulation of scenario 2, according to the field survey.

Crop parameters	scrubland	meadow	HCG	MCG	barren land
Surface Fraction (%)	50	100	100	35	-
Root Depth (cm)	150	10	50	30	-
Crop height (cm)	61	4.2	7	5	-
LAI	3.6	3.2	2.6	0.7	-
Interception threshold (mm) [a]	2.1	1.95	1.68	0.59	-
Interception constant (mm)	0.58	0.61	0.65	0.84	-

[a] the interception threshold is obtained from results of literatures in Qilian Mountain. The result for scrubland is from Liu et al., 2012 while meadow and grassland (HCG and MCG) are from Liu et al., 2013. Interception constant is obtained by dividing the daily interception thresholds by LAI (Wang et al., 2018). HCG and MCG represent high coverage grassland and medium coverage grassland, respectively.

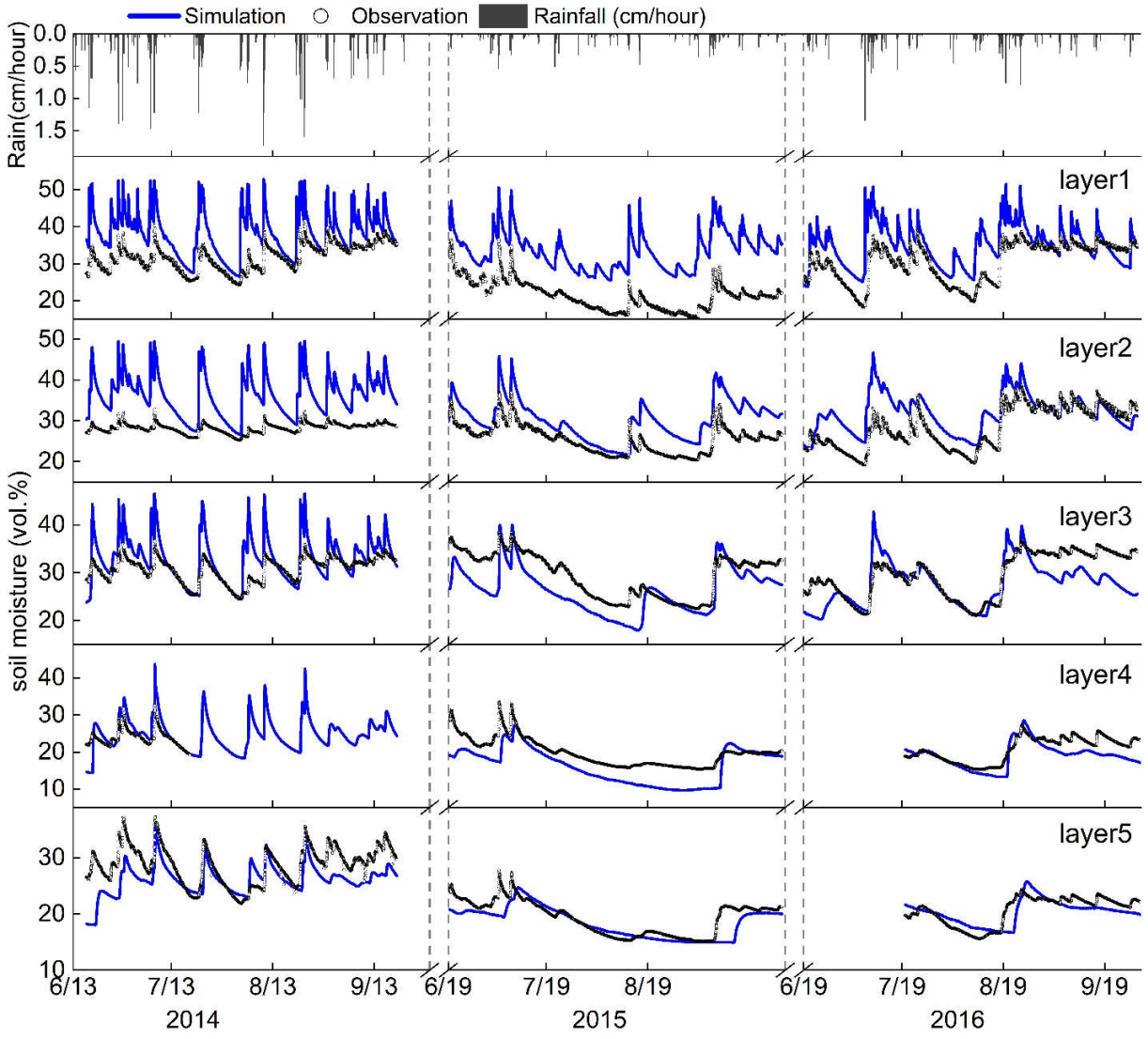

Fig. A1. The comparison of the observed and the simulated profile soil moisture of the scrubland soil moisture station during the growing season of 2014-2016.

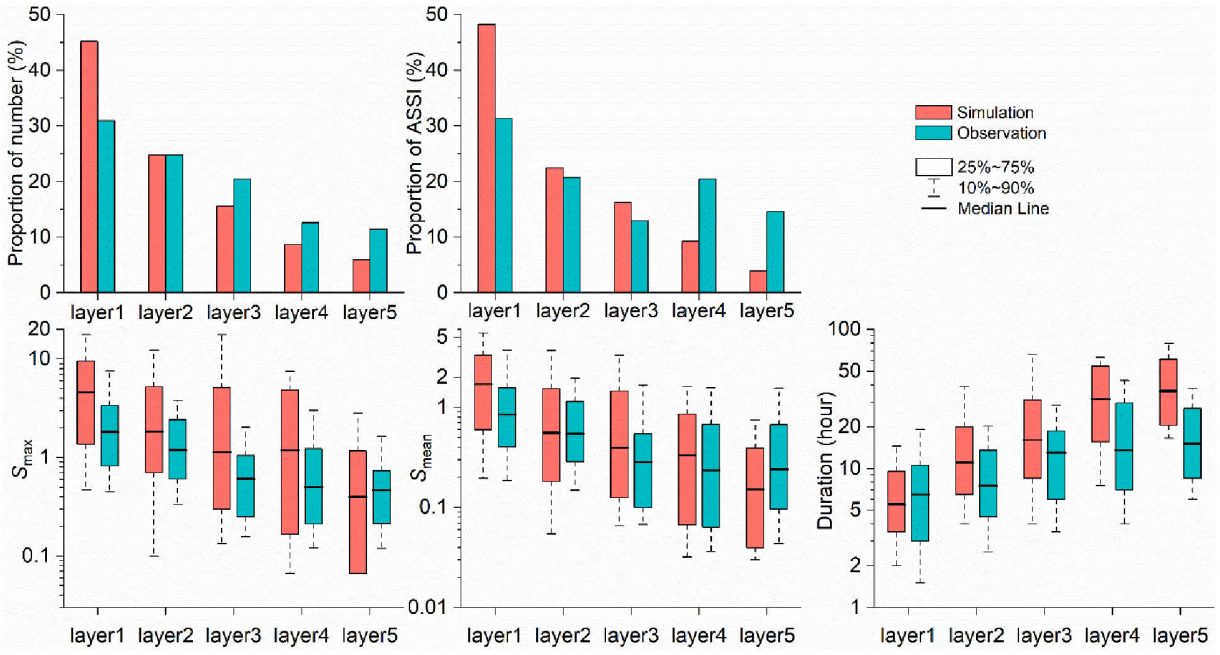

Fig. A2. Comparison of simulated and observed soil wetting events (SWE): the profile distribution of the proportion of SWE number and ASSI, S_{max}, S_{mean} and Duration. The boxplots for the S_{max}, S_{mean} and Duration are lognormal distribution to clearly display the entire distribution of the data. ASSI is the accumulated soil storage increment during the growing season of 2014-2016.

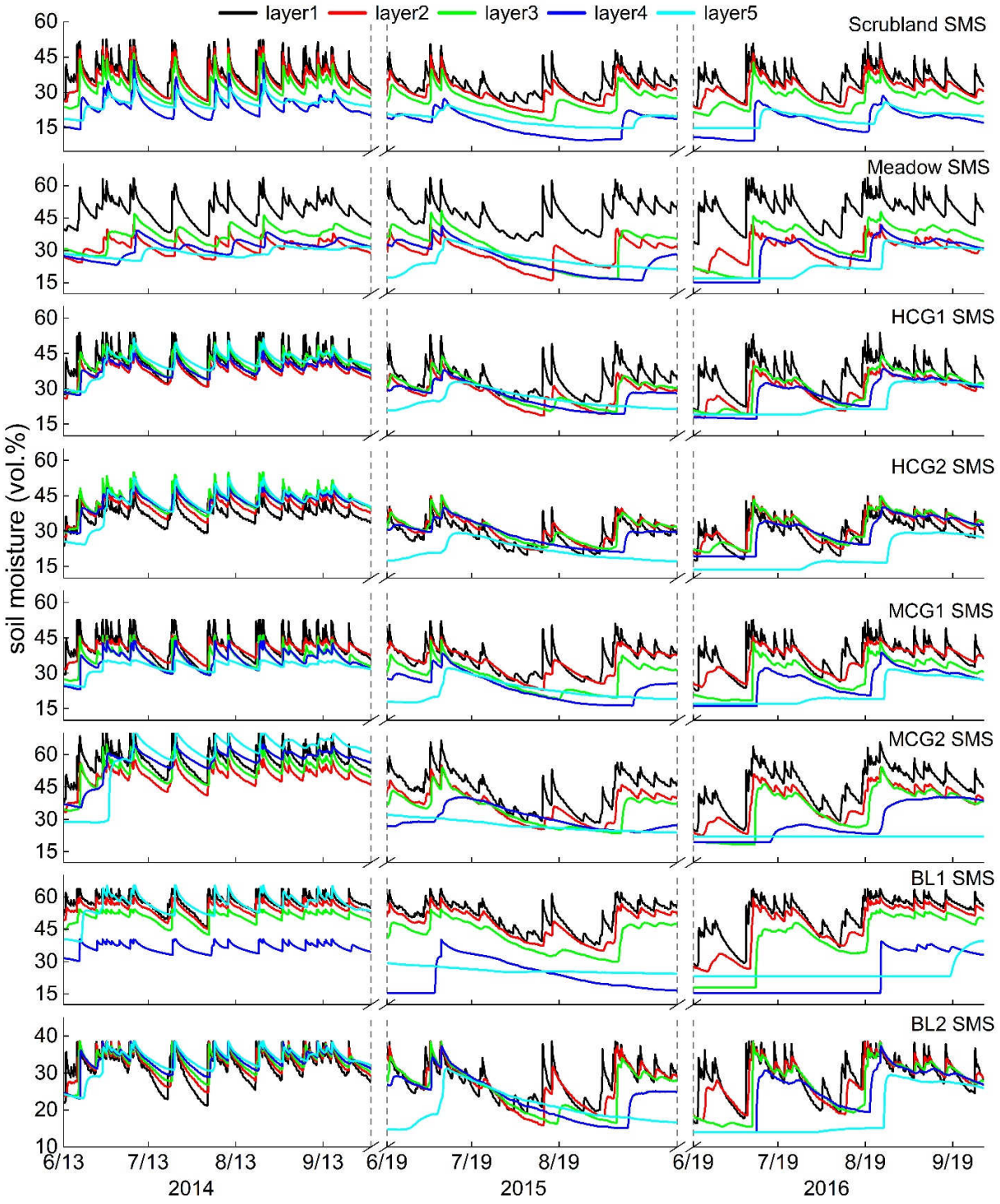

Fig. A3. The simulated soil moisture during the growing season of 2014-2016 under the condition of different profile soil properties with the same plant parameters to test the influence of soil property on the pattern of soil moisture dynamics. X axis is date, y axis is soil moisture (vol. %).

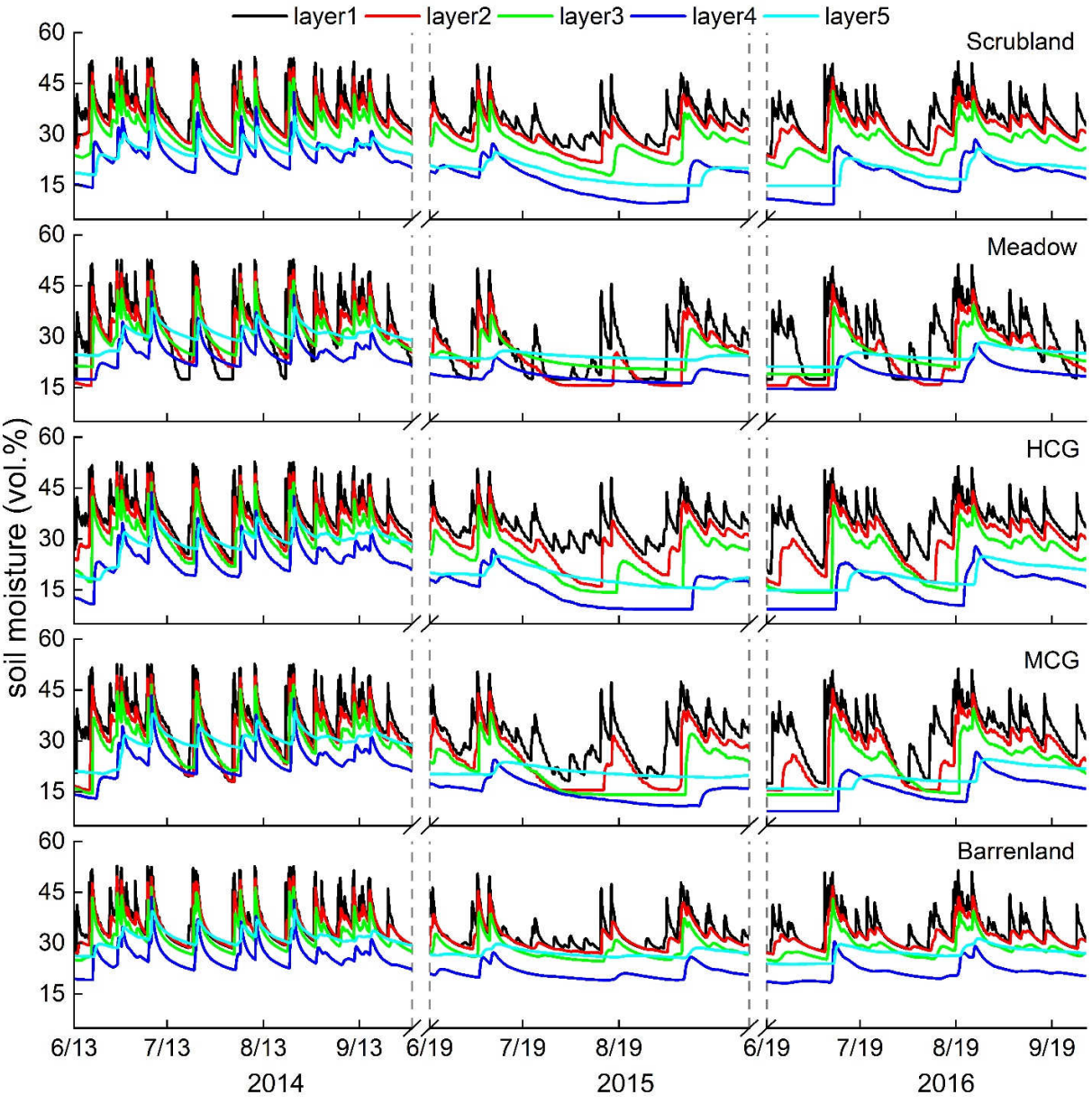

Fig. A4. The simulated soil moisture during the growing season of 2014-2016 under the condition of different plant parameters with the same profile soil hydraulic properties (same as the scrubland station) to test the influence of plant parameters on the pattern of soil moisture dynamics. HCG and MCG represent high coverage grassland and medium coverage grassland, respectively.

33 Reference

34 Liu, Y.Y., Peng, H.H., Meng, W.P., Bie, Q., Wang, Y., Zhao, C.Y., 2013. Artificial rainfall
35 interception characteristics in alpine meadows under diferent grazing scenarios in the upper
36 reach of Heihe River. J. Lanzhou Univ. Nat. Sci. 49 (6), 799-806 (in Chinese).
37 Liu, Z., Chen, R., Song, Y., Han, C. 2012. Characteristics of rainfall interception for four typical
38 shrubs in Qilian Mountain. Acta Ecol. Sin. 32 (4), 1337-1346 (in Chinese).
39 Wang, H., Tetzlaff, D., Soulsby, C. 2018. Modelling the effects of land cover and climate change
40 on soil water partitioning in a boreal headwater catchment. J. Hydrol. 558, 520-531.